Air Force Institute of Technology

AFIT Scholar

12-1999

Evaporation of Jet Fuels
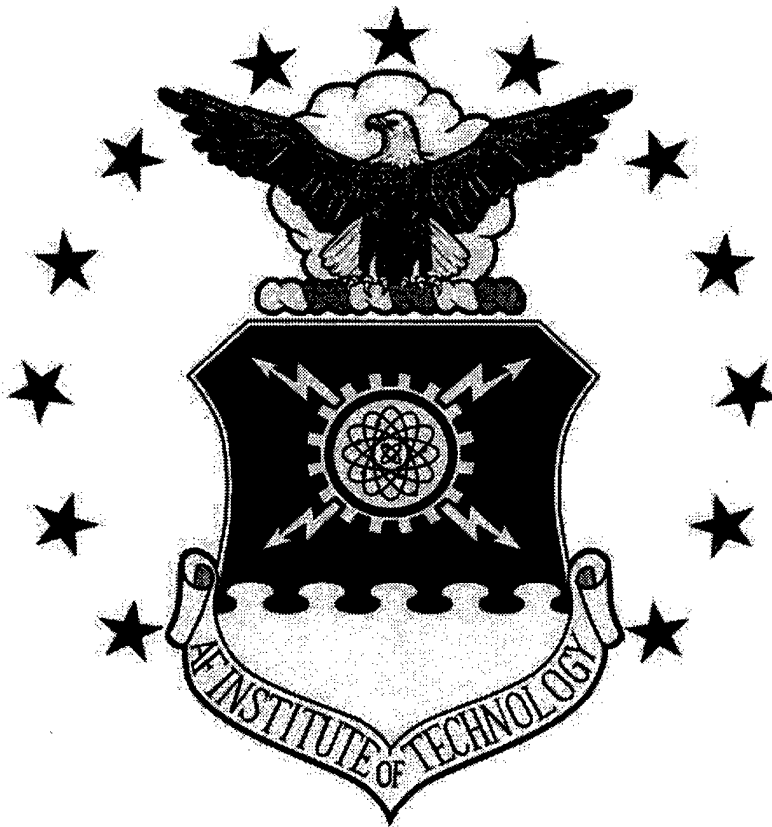
Charles Eric Hack

Follow this and additional works at: https://scholar.afit.edu/etd

Part of the Applied Mathematics Commons, and the Environmental Monitoring Commons

---

Recommended Citation

Evaporation of Jet Fuels

THESIS

Charles Eric Hack
AFIT/GES/ENC/99S-01

DEPARTMENT OF THE AIR FORCE
AIR UNIVERSITY
AIR FORCE INSTITUTE OF TECHNOLOGY

Wright-Patterson Air Force Base, Ohio

Evaporation of Jet Fuels

THESIS

Charles Eric Hack

AFIT/GES/ENC/99S-01

The views expressed in this thesis are those of the author and do not reflect the official policy or position of the Department of Defense or the United States Government.

Evaporation of Jet Fuels

THESIS

Presented to the Faculty of the AFIT School of Engineering

of the Air Force Institute of Technology

Air University

In Partial Fulfillment of the

Requirements for the Degree of

Master of Science in Environmental Science

Charles Eric Hack

September 1999

Evaporation of Jet Fuels

Charles Eric Hack

Approved:

(signature)   28 SEPT 1999

Dr. Dennis Quinn   Date
Thesis Advisor

(signature)   28 Sept 1999

Dr. Mark Goltz   Date
Committee Member

(signature)   28 Sept 1999

Dr. Larry Burggraf   Date
Committee Member

Acknowledgements

I would like to thank my thesis advisor, Dr. Dennis Quinn, for his assistance and guidance throughout this research effort. His advice and insights have helped me to develop as a scientist.

I would also like to thank Dr. Mark Goltz and Dr. Larry Burggraf for their valuable reviews and feedback on this thesis. Their inputs led to several improvements to this project and to a better thesis.

I thank the faculty of the math department. On several occasions, they listened to the difficulties that I was having with the research and offered excellent suggestions.

Finally, I am grateful to my wife, Teresa. She has given me support and encouragement, and remained confident in me throughout this experience. Her patience and love have been essential to completion of this thesis.

Charles Eric Hack

Table of Contents

List of Figures

vii

List of Tables

Abstract

Determining the fate and transport of JP-8 jet fuel is a complex and important problem. As part of the startup procedures for jet engines, fuel is passed through aircraft engines before combustion is initiated. Because of the extremely low temperatures at northern tier Air Force bases, the unburned fuel does not evaporate readily and may come into contact with ground crew. To determine the amount and duration of contaminant contact, the evaporation of the emitted fuel must be modeled. The amount and composition of the fuel upon reaching the ground crew may be determined by droplet evaporation models that have already been developed. The evaporation of the fuel after adhering to the skin needs to be modeled. This knowledge of the fuel's fate may then be used to determine source terms for use in toxicological studies.

This research involves the comparison of two existing droplet evaporation models and the calculation of the evaporation of a film of jet fuel from a surface. The existing models are compared in order to make recommendations on which model to use to predict the amount and composition of fuel reaching the ground crew. To make the surface evaporation problem amenable to modeling, simplifying assumptions are made. The fuel is assumed to be a uniformly distributed mixture of representative hydrocarbon groups. Due to the complexity of the mixture of aviation fuels, a mixture of the predominant species were chosen as representatives to approximate the physical behavior of the entire fuel mixture.

The goal of this research is to determine the most appropriate model for predicting the amount and composition of jet fuel reaching the ground crew and to extend the more appropriate fuel droplet evaporation model to describe the evaporation of a film of fuel from a surface. A validation of the resultant model is then performed by comparing the calculations to experimental data.

Evaporation of Jet Fuels

I. Introduction

1.1 Overview

Determining the fate and transport of JP-8 jet fuel is a complex and important problem. Normal air force operations sometimes require fuel to be released into the atmosphere. Fuel is purposely jettisoned from aircraft during emergency situations to reduce the risk of fire or to make it easier to land safely. Fuel is also passed through aircraft engines without combustion in order to prepare for flight.

Previous research into the evaporation and settling to the ground of jettisoned fuel has led to the development of two droplet evaporation and transport models to determine the amount and concentration of contaminant that reaches the ground after jettisoning. This knowledge of the fuel's fate has been used to determine minimum altitudes for jettisoning without contamination of the ground.

More recently, there have been reports of ground crews being exposed to unburned fuel during the cold start of jet engines at northern tier Air Force bases. Fuel is passed through the aircraft engines to prepare for flight. When the ambient temperature is extremely low, as it is at northern tier Air Force bases, the fuel does not evaporate quickly. The amount and composition of fuel reaching the ground crew can be predicted using existing droplet evaporation models (3), (16). However, there is a requirement to model the evaporation of the fuel from the ground crew's skin and clothing. The evaporation data could then be used to determine source terms for use in toxicological and pharmacokinetic studies such as determining the amount of fuel that is absorbed through the skin. Integrating models of evaporation

and absorption of the fuel through skin may then provide a quantification of the extent of exposure to the ground crew.

1.2 Problem

In order to assess the exposure of the fuel on the contacted ground crew, evaporation calculations are needed. It is unclear whether or not the several droplet evaporation algorithms that have been developed produce equivalent results. Comparisons must be performed to determine if there is a significant difference in the calculations and to determine which model should be used to predict the amount and composition of fuel reaching the ground crew. The ease of application of these models to newly developed fuels also needs to be considered as the fuel used by the Air Force is continually changing.

The fuel will not likely consist of spherical droplets after adhering to an object. Therefore, droplet evaporation studies that assume spherical droplets are not applicable to the fuel after it reaches the crew.

1.3 Scope

The scope of this research involves the numerical computation of the evaporation of a film of jet fuel from a surface and the comparison of existing fuel droplet evaporation descriptions. The droplet evaporation calculations will be examined in an attempt to determine which model should be used to predict the amount and composition of the fuel that reaches the ground crew. The surface evaporation calculation will be based on the previous studies of droplet evaporation. The droplet evaporation models will be modified as necessary to describe the evaporation of the fuel from a flat surface.

The fuel is assumed to be a uniformly distributed mixture of representative hydrocarbon groups. Due to the complexity of the mixture of aviation fuels, a mixture of the predominant species were chosen as representatives to approximate

1-2

the physical behavior of the entire fuel mixture. The evaporation of the fuel is complicated by the fact that the composition of the droplet is continually changing because the more volatile components evaporate more quickly than the less volatile components. Furthermore, the temperature of the fuel is continually changing which affects the evaporation rate. The fuel temperature approaches equilibrium with the ambient air temperature and is simultaneously cooled through evaporative cooling. These complications lead to a nonlinear system of equations describing evaporation that must be solved numerically.

1.4   Summary of Thesis

The thesis is organized as follows: Chapter 1, Introduction; Chapter 2, Background of evaporation theory; Chapter 3, Comparison of droplet evaporation algorithms; Chapter 4, Surface evaporation algorithm; Chapter 5, Conclusions and Recommendations; Bibliography.

II. Background

2.1 Overview

Evaporation is a heat and mass transport phenomenon. Thus, in order to understand and predict rates of evaporation, one must understand the rates associated with these processes. In the following sections, heat and mass transfer equations that describe evaporation of a liquid mixture are developed. The equations presented in the droplet evaporation descriptions begin with expressions for the time derivatives of droplet or species mass, temperature, and radius. The heat and mass transfer equations are presented here in order to illustrate that the calculations of droplet evaporation are derived from first principles. Following the development in section 2.2, the droplet evaporation calculations are presented and are referenced to the equations in section 2.2.

The principal references used for the heat and mass transfer rates presented in section 2.2 are Bird, Stewart, and Lightfoot(1) and Incropera and De Witt(7). Supplemental material is also taken from Clark(2) and Fuchs(5). The principal references for the theory applied in the combustion model are Glassman(6), Kuo(8), and Williams(18).

2.2 Physics of Evaporation

2.2.1 Mass Transfer.

2.2.1.1 Definition of Terms.
We begin by defining the concentrations, velocities, and fluxes that will be used to develop the mass transfer equation.

The fuel is composed of several components that we refer to as species. The concentration of species i may be expressed in several ways. The mass concentration, ρ_i, is the mass m of species i per unit volume of solution V. The molar concentration, $c_i = \rho_i/w_i$, where w_i is the molecular weight of species i, is the number of moles per

unit volume of solution. The mass fraction, $y_i = \rho_i/\rho$, is the mass concentration of i divided by the density of the solution. The mole fraction, $\chi_i = c_i/c$, is calculated as the molar concentration of i divided by the total number of moles per unit volume of solution, c.

Likewise, the velocity of a species moving through a solution may be expressed in different ways. Here, it is defined in terms of the mass because we want an expression for the mass flux. The velocity refers to the sum of the velocities of all molecules of a species divided by the total number of the molecules in a small volume. The mass average velocity, $\mathbf{v}$, of a mixture of N species is defined by:

$$\mathbf{v} = \frac{\sum_{i=1}^{N} \rho_i \mathbf{v}_i}{\rho} \tag{2.1}$$

where $\rho = \sum_{i=1}^{N} \rho_i$ is the total mass concentration.

The mass flux of species A relative to stationary coordinates is defined as:

$$\mathbf{n}_A = \rho_A \mathbf{v}_A, \tag{2.2}$$

The mass flux of A relative to coordinates moving at the average mass velocity of the mixture is defined as:

$$\mathbf{j}_A = \rho_A (\mathbf{v}_A - \mathbf{v}) \tag{2.3}$$

Replacing $\rho_A \mathbf{v}_A$ in the definition of $\mathbf{j}_A$ with $\mathbf{n}_A$ results in:

$$\mathbf{j}_A = \mathbf{n}_A - \rho_A \mathbf{v} \tag{2.4}$$

Substituting the definition of $\mathbf{v}$ yields:

$$\mathbf{j}_A = \mathbf{n}_A - \rho_A \frac{\sum_{i=1}^{N} \rho_i \mathbf{v}_i}{\rho} \tag{2.5}$$

For a binary mixture composed of species A and B, we may use the definition of the mass fraction of species i, $Y_i = \rho_i/\rho$, and the definition the mass flux of species i, $\mathbf{n}_i = \rho_i \mathbf{v}_i$, to replace equation (2.5) with:

$$\mathbf{j}_A = \mathbf{n}_A - Y_A(\mathbf{n}_A + \mathbf{n}_B) \tag{2.6}$$

2.2.1.2 Mass Diffusion. To describe the diffusion of species A through the mixture, Fick's first law is applied to give the mass flux of A with respect to the mass average velocity:

$$\mathbf{j}_A = -\rho\mathcal{D}\nabla Y_A \tag{2.7}$$

where $\mathcal{D}$ is the diffusion coefficient and ∇Y_A is the concentration gradient of A. Notice that the sign of the right hand side of equation (2.7) is negative. That means that the mass will flow in the direction of steepest concentration descent. That is, A will move from an area of high concentration to an area of low concentration.

Rearranging equation (2.6) and replacing $\mathbf{j}_A$ using Fick's law yields:

$$\mathbf{n}_A = Y_A(\mathbf{n}_A + \mathbf{n}_B) - \rho\mathcal{D}\nabla Y_A \tag{2.8}$$

where $\rho\mathcal{D}\nabla Y_A$ is the contribution to the mass flux by ordinary diffusion and $Y_A(\mathbf{n}_A + \mathbf{n}_B)$ is the contribution due to the diffusion induced bulk movement of A and B. To see that the bulk contribution is physically sensible, consider what happens as A begins to evaporate and diffuse away from the surface. There is clearly a flux of A away from the liquid. If we assume that gas B is insoluble in liquid A, there also must be a flux of B away from the liquid as it moves to make room for the additional molecules of A. The result is a net flux of both A and B away from the surface.

Fick's law describes diffusion when there are no convective affects. This has application to problems where the medium through which A is diffusing is motionless.

To handle problems where the medium is in motion, we must consider mass transport by diffusion and convection.

2.2.1.3 *Mass Diffusion-Convection.* Consider mass transfer across a liquid-vapor phase boundary as in Figure 2.1 where liquid A is evaporating into a gas B, and gas B is moving with a constant velocity u.
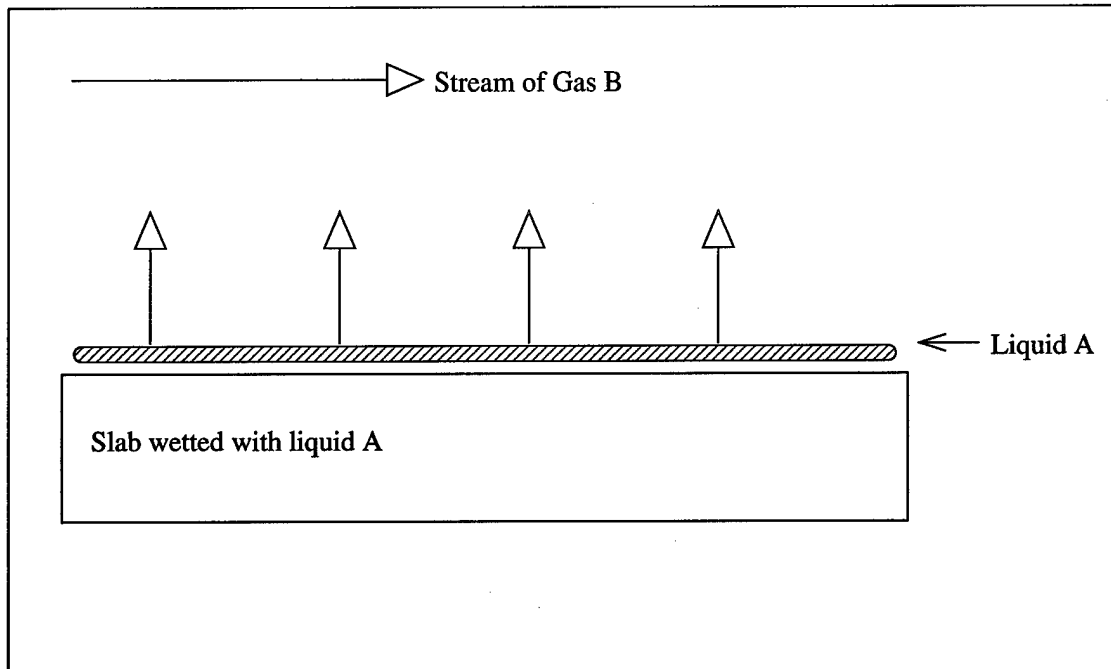
Figure 2.1   Depiction of evaporation process.

The motion of B across the surface causes convective mass transfer to occur in addition to the diffusion mass transfer. Problems of this sort are generally too complex to solve analytically. Instead, a mass transfer coefficient, k, is defined as in Bird(1) in terms of the rate of diffusion normal to the gas-liquid interface as follows:

$$j_{A0} = k\Delta Y_A \qquad (2.9)$$

where j_{A0} is the flux of gas A into the gas B at the liquid-vapor boundary, with the zero subscript to denote conditions at the liquid-vapor boundary, and ΔY_A is the

difference between the gas phase concentration of A at the liquid-vapor boundary and in the approaching stream of gas B. Here, k has been averaged over the surface area of the liquid A. Notice that the sign of the right hand side of equation (2.9) is positive because j_{A0} is the mass evaporating per unit area per unit time.

Evaluating equation (2.6) at the surface of the liquid, denoting this with a zero subscript, and rearranging results in:

$$n_{A0} = Y_{A0}(n_{A0} + n_{B0}) + j_{A0}$$

Substituting j_{A0} from equation (2.9) yields:

$$n_{A0} = Y_{A0}(n_{A0} + n_{B0}) + k\Delta Y_A \qquad (2.10)$$

where n_{A0} is the mass flux at the liquid surface with respect to fixed coordinates.

The mass transfer coefficient is an empirically derived parameter that represents all convective effects. At high mass transfer rates, the coefficient is dependent on the mass transfer rate since high rates may change the concentration profiles. However, for slow mass-transfer rates, such as those typical of evaporation processes, the concentration profile distortion is negligible. The coefficient also depends on the position on the boundary. However, since the usual value measured is the flux averaged over the entire surface area, this dependence is neglected so that measured values may be used.

Since k is a function of many properties of the fluid A and gas B, the expression for a particular geometry is usually found in terms of a smaller number of dimensionless parameters. For convective mass transfer between an object with a characteristic length scale L and a surrounding fluid, k is defined in terms of the Sherwood number, N_S, which is also called the Nusselt number for mass transfer. The Sherwood number is arrived at through dimensional analysis as in Bird (1) and

Clark (2). Previous researchers have noticed similarities between mass flux expressions derived for different problems with different geometries:

- The flux is proportional to a characteristic concentration difference.

- The flux is inversely proportional to the characteristic length scale, L.

- The flux is proportional to $\rho \mathcal{D}^p, 0.5 \leq p \leq 1$.

These three observations suggest that multiplying both sides of (2.9) by $L/(\rho \mathcal{D} \Delta Y_A)$ yields a dimensionless parameter group. This group is the Sherwood number or the Nusselt number for mass transfer, N_S:

$$N_S = \frac{j_{A0}L}{\rho \mathcal{D} \Delta Y_A} = \frac{kL}{\rho \mathcal{D}} \tag{2.11}$$

The Sherwood number is a dimensionless parameter that is obtained from experimental measurements. The form of the number is as a function of the Reynolds number, N_R, and the Schmidt number, N_c, and the geometry of the system:

$$N_S = f(N_R, N_c, \text{geometry})$$

where the Reynolds number is defined as

$$N_R = \frac{Lu\rho}{\mu}$$

and the Schmidt number is the defined as

$$N_c = \frac{\mu}{\rho \mathcal{D}}$$

where u is the object's mean velocity relative to the surrounding fluid, ρ is the density of the fluid, and μ is the absolute viscosity of the fluid. Notice that the Schmidt number has $\rho \mathcal{D}$ in the denominator. This is where the exponent p comes from in the observation that the flux is proportional to $\rho \mathcal{D}^p$.

By multiplying the Reynolds number by u/L^2, we realize its physical significance:

$$N_R = \frac{\rho u^2/L}{\mu u/L^2} = \frac{Lu\rho}{\mu} \tag{2.12}$$

This is the ratio of inertial to viscous forces.

We obtain the mass transfer coefficient by solving (2.11) for k which yields:

$$k = \frac{\rho \mathcal{D} N_S}{L} \tag{2.13}$$

Now that we have the basic equations needed to describe evaporation, consider the evaporation of a spherical droplet of A in a motionless surrounding fluid B. Notice that in spherical coordinates, the net bulk flow induced by ordinary diffusion in (2.10) is zero. This results in the equality of n_{A0} and j_{A0}. Thus:

$$j_{A0} = n_{A0} = k\Delta Y_A \tag{2.14}$$

For sufficiently small Δt, the mass of the droplet lost during time Δt is the rate of the mass crossing the surface times Δt:

$$m(t + \Delta t) - m(t) = \pi D^2 j_{A0} \Delta t \tag{2.15}$$

where D is the diameter of the sphere and πD^2 is the surface area of the sphere. Dividing both side of (2.15) by Δt and taking the limit as $\Delta t \to 0$ results in the instantaneous evaporation rate:

$$\frac{dm}{dt} = \pi D^2 j_{A0} \tag{2.16}$$

where j_{A0} is the rate of mass flow per unit area of A across the surface of the sphere. Replacing j_{A0} with the expression in (2.14) results in:

$$\frac{dm}{dt} = \pi D^2 k \Delta Y_A \qquad (2.17)$$

The concentration gradient is taken to be $\Delta Y_A = Y_{A0} - Y_{A\infty}$, the difference between the gas phase concentration of A at the surface and the concentration of A in the approaching gas B. Assume that the gas concentration of A at the surface of the droplet is equal to the equilibrium concentration and that the ambient concentration of A is zero which results in $\Delta Y_A = Y_{A0}$. Then, substituting k from equation (2.13), the change in mass becomes:

$$\frac{dm}{dt} = \pi D^2 Y_{A0} \frac{\rho \mathcal{D} N_s}{D} \qquad (2.18)$$

where the characteristic length scale is D and the empirical relation for the Sherwood number for a sphere surrounded by a flowing fluid is given by:

$$N_S = 2.0 + 0.60 N_R^{1/2} N_c^{1/3} \qquad (2.19)$$

Notice that the product $\rho\, Y_{A0}$ is the mass concentration of A at the phase boundary, ρ_{A0}, and $\rho_{A0} = c\, w_A\, \chi_{A0}$ where c is the total molar concentration, w_A is the molecular weight of species A, and χ_{A0} is the gas phase mole fraction of species A at the surface. These quantities are more easily calculated than ρ_{A0}. Then, the evaporation rate becomes:

$$\frac{dm}{dt} = \pi D c w_A \chi_{A0} \mathcal{D} N_S \qquad (2.20)$$

From the ideal gas law, we have

$$c = n/V = P/(RT), \qquad (2.21)$$

where P is pressure, V is volume, n is the number of moles of gas, R is the universal gas constant, and T is the temperature. If we assume that A and B form an ideal gas mixture, then $c = n/V = P/(RT)$ which yields:

$$\frac{dm}{dt} = \pi D w_A \chi_{A0} \mathcal{D} N_S \frac{P}{RT} \tag{2.22}$$

If the gas phase concentration at the surface is the equilibrium concentration, the mole fraction is equal to the vapor pressure , P^v, divided by the total pressure. Substituting the expression $\chi_{A0} = P_A^v/P$ into (2.22), the instantaneous evaporation rate of A is given by:

$$\frac{dm}{dt} = \pi D \frac{N_S \mathcal{D} w_A}{RT} \frac{P_A^v}{} \tag{2.23}$$

Since $N_S = 2$ when the relative droplet velocity is zero, this expression is equivalent to Maxwell's equation for the evaporation of droplets with zero velocity with respect to the surrounding fluid (see equation (1.14) in reference(5)).

2.2.2 Heat Transfer. There are several mechanisms of heat transport. For the evaporation problem, we must consider heat transfer between an object and a surrounding fluid as a result of conduction, convection, and radiation. The principal references for the equations describing these mechanisms of heat transport are Bird, Stewart, and Lightfoot (1) and Incropera and DeWitt (7).

When evaporation occurs, heat is lost through evaporative cooling. Although the heat is not directly transferred to the surrounding fluid, it is presented here since it effects the temperature of the evaporating liquid.

2.2.2.1 Heat Conduction. Heat conduction is the transfer of heat through a stationary medium due to a temperature gradient. The mechanism of conduction is molecular or atomic activity where heat is transferred from particles with high energy to particles with lower energy.

Fourier's Law quantifies the rate of heat transfer by conduction:

$$\mathbf{q} = -\kappa \nabla T \qquad (2.24)$$

where $\mathbf{q}$ is the heat flux, κ is the thermal conductivity, and ∇T is the temperature gradient. It states that the heat transfer per unit time per unit area is proportional to the temperature gradient. Note that the heat flows in the direction of steepest temperature descent.

Note the similarity of equation (2.24) with equation (2.7). We will see that the similarities between mass and heat transfer will carry through the discussion heat convection as well. The empirical relationship for the heat transfer coefficient is analogous to that for the mass transfer coefficient where the Sherwood number is replaced by the Prandtl number and the $\rho \mathcal{D}$ product replaced by the thermal conductivity. In fact, the mass transfer coefficient is often deduced by making an analogy to the corresponding heat transfer coefficient and performing the replacements just stated.

2.2.2.2 Heat Convection. Heat convection is the heat transfer between an object and a flowing medium. It is composed of two mechanisms, conduction and advection. For example, consider a fluid flowing over a heated surface as in figure 2.2. Because of friction between the fluid and the surface, the velocity of the fluid varies from 0 to u throughout a region called the hydrodynamic boundary layer. The temperature also varies in a region called the thermal boundary layer, from T_s at the surface to T_∞, the ambient fluid temperature. The heat is moving away from the surface because the surface is being heated to a higher temperature than the fluid. It is a result of both conduction to the boundary layer due to a temperature gradient, and the bulk flow carrying heated fluid away.
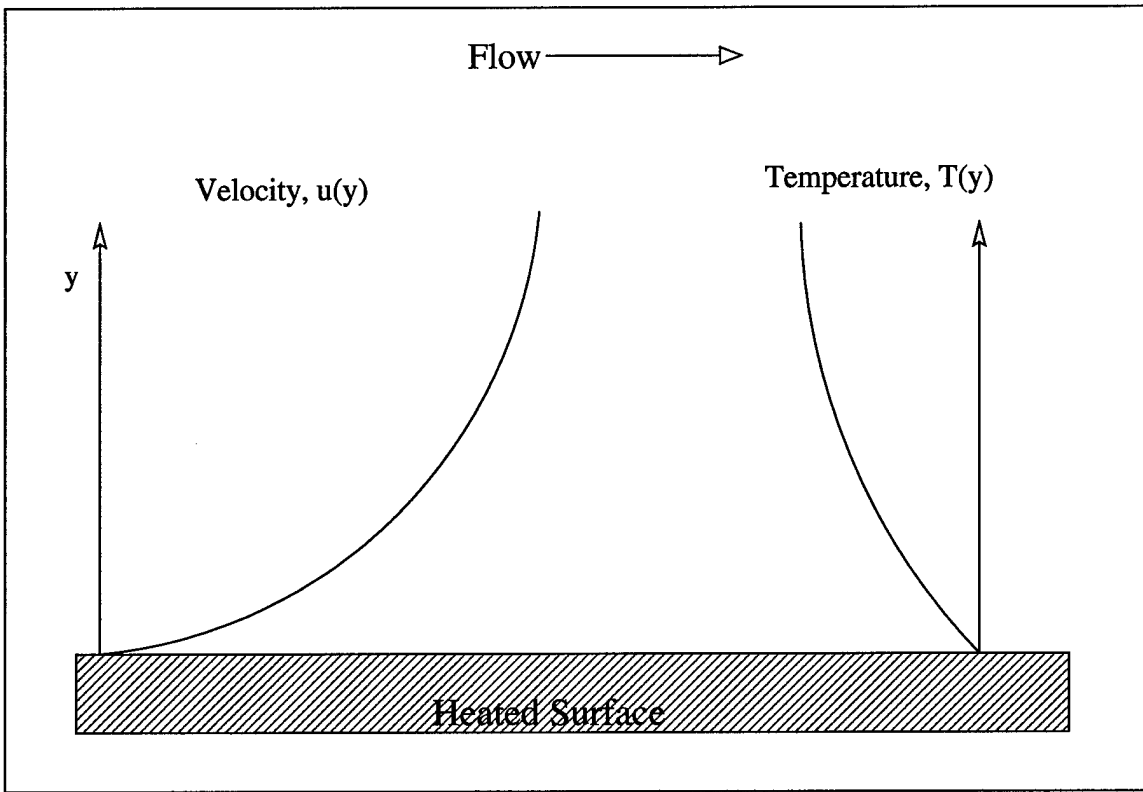
Figure 2.2   Velocity and temperature profiles in the heat transfer to a fluid flowing over a heated surface.

There are two limiting types of heat convection, free and forced convection. Although most processes are placed into one of the two categories, it is possible for both types of convection to be significant simultaneously.

Forced convection occurs when the object is in motion with respect to the surrounding medium, as in the example of figure 2.2. The fluid is heated by the object and then carried away by some external force such as gravity pulling an object through the air or a fan.

Free convection occurs when the surrounding fluid is set into motion by density differences. As the fluid is heated by the object, it becomes less dense. The medium will then move due to increased buoyancy. The result is a net transport of heat away from the object called free convection. In the example of figure 2.2, if $u \to 0$, then we would have free convection. The density of the fluid above the surface would begin decrease as it was heated by the surface. This would cause the fluid near the surface to rise and be replaced with cooler fluid. As the heated fluid rises, it transports heat away from the surface.

For either type of convection, Newton's law of cooling relates the convective heat flux to the temperature gradient:

$$\mathbf{q}_c = h \nabla T \tag{2.25}$$

where $\mathbf{q}_c$ is the convective heat flux, ∇T is the temperature gradient, and h is the convection heat transfer coefficient. The heat transfer coefficient depends on the boundary layer conditions, which are influenced by the object's geometry and several of the fluid properties such as the viscosity, density, heat capacity, etc.. For complex situations involving object-fluid boundaries and convective transport, the heat transfer coefficient, like the mass transport coefficient, must be fitted to experimental data. By making an analogy to convective mass transport, the empirical

relationship for the heat transfer coefficient is defined as:

$$h = \frac{\kappa N_u}{L},$$

(2.26)

where Nu is the Nusselt number for heat transfer, and L is the characteristic length of the object. The empirical relationship for N_u is analogous to that for N_S:

$$N_u = f(N_R, N_P, \text{geometry})$$

where $N_P = \mu C_p/\kappa$ is the Prandtl number, the heat transfer analog to the Schmidt number, μ is the fluid viscosity at the surface and C_p is the gas phase, constant pressure heat capacity of the fluid at the surface.

For convective heat flux between a spherical droplet and a surrounding fluid, the Nusselt number is given by a relationship similar to that for the Schmidt number:

$$N_u = 2.0 + 0.6 N_R^{1/2} N_P^{1/3}$$

If we also assume that we have spherical symmetry, then $\nabla T = dT/dr$ which is set equal to $T_s - T_\infty$. The heat flux normal to the droplet surface from the surrounding fluid is then:

$$q_c = \frac{\kappa}{D}(2.0 + 0.6 N_R^{1/2} N_P^{1/3})(T_s - T_\infty)$$

(2.27)

where q_c is the radial heat flux through conduction with convection and the droplet diameter D is the characteristic length scale.

2.2.2.3 Heat Radiation. For the range of magnitudes for the temperature gradient between the atmosphere and either a released droplet or the resultant film of fuel, heat transfer by radiation will be small relative to convective transfer. However, it is presented here for completeness because it is incorporated into previous work.

The principles of radiative transfer are derived from the analysis of black bodies, objects for which absorptivity is unity over all wavelengths and temperatures. The absorptivity a is defined as the ratio q^a/q^i, where q^a is the flux of energy absorbed and q^i is the incident flux of energy. Any real body will have absorptivity less than unity.

The total energy emitted by a black body, q_b^e, is given by the Stefan-Boltzmann law:

$$q_b^e = \sigma T^4 \tag{2.28}$$

where σ is the empirically derived Stefan-Boltzmann constant and T is the temperature in Kelvin. With the exception of fluorescent bodies, the energy emitted by real, nonblack bodies will be less than indicated in (2.28). How much less is characterized by the emissivity of the object e, which is defined as:

$$e = \frac{q^e}{q_b^e} \leq 1 \tag{2.29}$$

where q^e without the subscript b is the energy emitted by the nonblack body. Therefore, the energy emitted by a real body is given by:

$$q^e = e\sigma T^4 \tag{2.30}$$

To quantify the radiant energy transfer between two bodies, we must consider only the radiation directed at the bodies. To see this is not necessarily the same as the total energy emitted, consider the transfer between two spheres separated by a vacuum. Although energy is radiated from the entire surface of a body, only that which is directed at the other body contributes to any exchange.

When an object is surrounded by a fluid, however, all of the energy radiating from the object is directed toward the surrounding fluid and we can simply use

(2.30). The net flux of energy from the object to the surrounding fluid is then:

$$q_r = \sigma(e_s T_s^4 - a_s T_\infty^4) \qquad (2.31)$$

where e_s is the emissivity of the object, T_s is the temperature of the object, a_s is the absorptivity of the object, and T_∞ is the temperature of the fluid.

2.2.2.4   Evaporative Cooling.   There is a certain amount of heat energy, called the heat of formation, associated with each of the three phases, solid, liquid, and gas. When a substance moves from one phase to another, there is a change in heat. The change in heat that occurs when a substance moves from liquid to gas is quantified by the latent heat of vaporization, ΔH_{vap}. The latent heat of vaporization gives the amount of heat lost per unit mass of the substance that is vaporized. Thus, the flux of heat due to evaporative cooling, q_h is given in term of the change in mass as:

$$q_h = \frac{\Delta H_{vap}}{A} \frac{dm}{dt} \qquad (2.32)$$

where A is the surface area of the evaporating liquid which is in the denominator in order to be consistent with units of the previous modes of heat flux, conduction, convection, and radiation.

2.3 Existing Droplet Evaporation Models

2.3.1 Overview. The evaporation of jettisoned jet fuels has been studied for several decades. In particular, two efforts have led to the publishing of fuel evaporation descriptions to predict the fate of jettisoned fuel from aircraft. Each investigation is based upon different approaches to the problem.

The first approach was developed by Lowell at NASA(10). It can be shown that Lowell's approach is based on the heat and mass transfer principles presented in section 2.2. Lowell's work was further improved by Clewell(3), followed by Pfeiffer, Quinn, and Dunge at AFIT(13). The advances in the dispersion modeling of jettisoned fuel are presented here because they must be used to determine the initial amount of fuel reaching the ground crew.

The second approach of Runge et al. (16) is based on Williams'(18) and Law's(9) work on droplet combustion.

The assumptions and equations of the two approaches are presented in this chapter. As they are presented, the equations of section 2.2 are referenced to demonstrate the scientific foundations of the models. This knowledge of the principles incorporated will make it possible to determine what modifications must be made to extend the equations to describe the evaporation of fuel from a non-spherical surface.

2.3.2 Lowell, Clewell, and Pfeiffer. Lowell developed a description of the evaporation and dispersion of jettisoned JP-4 (10) and JP-1 (11) jet fuel. For the JP-4 model, the droplet temperature was assumed to always equal the ambient temperature to simplify the calculation. For his later research on the less volatile JP-1, he included a droplet cooling calculation and an adaptive time step. The adaptive time stepping scheme increased the time step if the evaporation rate was small. Lowell established upper bounds on the amount of mass evaporated and distance fallen during a time step. If the upper bounds are exceeded, the time step

is shortened to maintain the accuracy of the approximate solution. This scheme significantly reduces the computational time of the simulation.

Jet fuel is a very complex mixture of hydrocarbons and to characterize the evaporating substance perfectly is not practical. Furthermore, variations in the refining process result in variations in the composition of the fuel. Therefore, the fuel has been characterized by a mixture of a finite number of species that approximate the physical behavior of the actual compounds in the mixture. The individual fuel species are characterized by the volume fraction, molecular weight, boiling point, and reference density at 20 degrees Celsius. The characterization developed by Lowell used only a 10 component characterization of the fuels.

Lowell also developed a dispersion model to determine the concentration of the fuel. He characterized the jettisoned plume as an infinite line source and calculated a minimum altitude for jettisoning at which the fuel presented no fire hazard. Lowell noted, however, that further study was needed to predict ground contamination by the jettisoned fuel.

Clewell's study (3) is an improvement of the work of Lowell to predict the evaporation of jettisoned aircraft fuel. Clewell's model is refined by the inclusion of experimental data provided by the Arnold Engineering Development Center (AEDC), an initial droplet temperature estimate based on the speed of the jettisoning aircraft, and a more detailed fuel characterization with 33 components for JP-4 and 27 components for JP-8. The more complete fuel characterization allows the model to simulate 99.9% evaporation of the initial mass.

Clewell developed a simpler dispersion model than Lowell's to use with the evaporation model to predict ground contamination by the fuel. Although his dispersion box model was less accurate than Lowell's infinite line source, Clewell was able to use it to get an upper bound on the amount of ground contamination.

Pfeiffer's work, while at the Air Force Institute of Technology (AFIT), was based on the evaporation equations of Lowell and Clewell. He improved the description by with a more accurate Gaussian dispersion model and by incorporating of actual upper atmosphere data obtained from several hundred stations worldwide that report vertical profiles of temperature, humidity, pressure, and wind velocity. This more accurate atmosphere characterization leads to major improvement in the model's accuracy as far as fuel jettisoning is concerned. This more accurate dispersion model is a significant improvement in predicting the concentration of fuel upon reaching the ground crew (13, 12).

2.3.2.1 Assumptions.

1. Quasi-steady state evaporation. The droplet diameter is fixed at each time step and then updated after the new mass and temperature are calculated.

2. The droplet falls at the terminal velocity for its current diameter, density, and altitude.

3. Raoult's law applies.

4. Each component evaporates independently of the rest of the mixture.

5. The initial fuel temperature is equilibrated with the temperature of the skin of the aircraft.

6. The atmosphere is standard. This assumption does not have to be made if the actual profiles are obtained.

7. The mixture is ideal so that the droplets volume is the sum of the volumes of the components. This assumption closely approximates the actual solution because all of the components of the mixture are hydrocarbons.

2.3.2.2 Model Equations. Following Clewell (3), the evaporation rate of the ith component is:

$$\frac{dm_i}{dt} = \pi D^2 k_i P_i^v, \qquad i = 1..N \qquad (2.33)$$

where k_i is the mass transfer coefficient of component i and is given by:

$$k_i = \frac{N_{s,i} \mathcal{D}_i w_i}{DRT_\infty} \qquad (2.34)$$

Notice that equation (2.33) is equivalent to equation (2.23) when we subscript the properties for a multicomponent mixture and thereby let the diffusivity $\mathcal{D}_i$ denote the multicomponent diffusivity.

When we assume Raoult's Law applies, the vapor pressure exerted by component i in a mixture is calculated using:

$$P_i^v = \chi_{i,\ell} P_i^{v,o} \qquad (2.35)$$

where $P_i^{v,o}$ is the pure liquid vapor pressure of component i, P_i^v is the pressure exerted by component i in a mixture, and $\chi_{i,\ell}$ is the mole fraction of species i in the liquid phase.

In equation (2.34), the subscript on the Sherwood number is necessary because it is a function of the Schmidt number, which is a function of the diffusivity of the ith component, $\mathcal{D}_i$:

$$N_{c,i} = \frac{\mu}{\rho \mathcal{D}_i} \qquad (2.36)$$

The diffusivity of component i in air is computed following Clewell who derived the expression from one given in Bird et al. (1):

$$\mathcal{D}_{i,a} = \frac{2.66 * 10^{-5} T_m^2 (1/w_i + 1/w_a)^{1/2}}{P_{atm}(V_b^{1/3} + 0.31)^2} \qquad (2.37)$$

where T_m is the mean of the droplet and ambient temperatures, V_b is the molar volume of component i at its normal boiling point, P_{atm} and the subscript a denotes air.

The differential equation is solved using a finite difference approximation of the time derivative to obtain a mass for the ith component of the fuel:

$$\Delta m_i = \pi D^2 k_i P_i \chi_{i,\ell} \Delta t, i = 1..N, \qquad (2.38)$$

where $\Delta m_i = m_i(t + \Delta t) - m_i(t)$, and Δt is the time step for the approximation which is adjusted as in Lowell's work(11).

The droplet's net rate of change in thermal energy, Q, is computed by performing an energy balance:

$$Q = \text{Heat in per unit time - Heat out per unit time}$$

Recall from equation (2.31) in section 2.2 that the flux of heat transferred to the droplet by radiation from the atmosphere is given by:

$$q_r = \sigma(a_d T_\infty^4 - e_d T_d^4)$$

where the subscript d denotes a property of the droplet.

From equation (2.27) in section 2.2, the flux of heat transferred to the droplet by conduction-convection is:

$$q_c = h \, \Delta T = h \, (T_\infty - T_d)$$

The Prandtl number and thermal conductivity used in the calculation of the heat transfer coefficient are assumed to be approximately those of air (3).

In addition, there will be a flux of heat loss by the droplet due to evaporative cooling that is given by equation (2.32) in section 2.2:

$$q_h = \frac{\Delta H_{vap} \frac{dm}{dt}}{A}$$

where dm/dt is the sum of the species evaporation rates, dm_i/dt.

Furthermore, if the fuel is jettisoned at high altitude, the droplet will be heated significantly by solar radiation. The flux of heat to the droplet by this mechanism is given by:

$$q_s = \frac{\hat{L}(1 - \alpha)}{4}$$

where α is the droplet's albedo and $\hat{L}$ is the solar insolation rate at altitudes typical of fuel jettisoning events. Clewell uses a rather high value of 1000 for the solar insolation rate to account for the high altitudes encountered. This value is not adjusted as the droplet falls.

Combining these relations into an energy balance by adding the heat transferred to the droplet and subtracting the heat loss by evaporative cooling results in the rate of heat transferred to the droplet:

$$Q = \pi D^2 (q_r + q_s + q_c - q_h) \tag{2.39}$$

where πD^2 is the surface area of the droplet and q_h is subtracted because it has been formulated in terms of the positive evaporation rate instead of the negative change in mass. Since Q is the change in energy per unit time, Q divided by $m \, c_\ell$ results in the change in temperature with respect to time:

$$\frac{dT_d}{dt} = \frac{Q}{mc_\ell} \tag{2.40}$$

The droplet surface temperature, T_d, is then calculated in one of two ways depending on whether the droplet is warmer or cooler than the ambient temperature. If the droplet is warmer than the ambient temperature, the droplet cooling is calculated by using a forward difference approximation to the derivative:

$$\Delta T_d = \frac{dT_d}{dt} \Delta t$$

If the droplet is cooler than the ambient air, a steady-state calculation is performed. The difference between the ambient and droplet temperature is calculated by setting $Q = 0$ and solving for the equilibrium temperature difference at the conditions for the current time step. Since this equation is nonlinear, a Newton-Raphson method is used to solve for the temperature iteratively:

$$T_{n+1} = T_n - \frac{Q(T_n)}{Q'(T_n)}, \tag{2.41}$$

where the prime denotes differentiation with respect to T. The initial guess is $T_0 = T(t)$ and the iteration continues until $T_{n+1} - T_n < 0.01$. If the temperature change calculated from (2.41) is too great, (2.38) is recalculated using the new temperature. This process is repeated until a steady state temperature is reached.

The droplet's altitude is updated by

$$H(t + \Delta t) = H(t) - \Delta H = H(t) - u(t)\Delta t \tag{2.42}$$

where $u(t)$ is the droplet's terminal velocity for its size at time t.

This algorithm incorporates an adaptive time step. The time step is adjusted based on the magnitude of the changes in mass and altitude. If either of the changes calculated in equations (2.38) and (2.42) are greater than their prescribed maximums, Δt is halved and Δm, ΔH, and ΔT are recalculated until the changes in the mass and altitude are below their maximums.

Once ΔH and Δm are within acceptable limits, droplet conditions are updated for use in the next iteration. If ΔH and Δm are now below their prescribed minimums, the time step is doubled and the calculation continues using the new droplet and ambient conditions as input for the next time step.

The droplet diameter is calculated from the new droplet volume as follows:

$$V_i = m_i / \rho_i \beta(T) \tag{2.43}$$

$$V_d = \sum_{i=1}^{N} V_i \tag{2.44}$$

$$D = (\frac{6}{\pi} V_d)^{1/3} \tag{2.45}$$

where $\beta(T)$ is a density correction factor to account for the temperature dependence of ρ, V_i is the volume that species i contributes to the total volume, V_d.

2.3.3 Runge, Teske, Polymeropolous. Two models are considered in this section, both of which are based on Law's rapid mixing model approach to describing combustion of fuels (9) as discussed in this section. The first model is found in a master's thesis by Runge (17). The second was presented in an article by Runge, Teske, and Polymeropolous (16).

To burn a single droplet of fuel, the condensed fuel must first be vaporized. Therefore, the rate at which a droplet burns is controlled by the rate of evaporation. For this reason, combustion models include a calculation of rates of evaporation. The system described here assumes a single, multicomponent fuel droplet evaporating in a quiescent atmosphere. The rate obtained through this analysis is then corrected for effects of convection using the methods as discussed in section 2.2.

2.3.3.1 Assumptions.

1. Spherical symmetric droplets with empirically corrected vaporization enhancement due to droplet motion.

2. Spatially uniform, temporally varying temperature and component concentrations in the droplet.

3. Raoult's law applies.

4. The thermal conductivity, λ, and gas and liquid phase specific heats, c_p and c_ℓ, are constant with respect to time and fuel component.

5. The Lewis number, $N_L = N_c/N_P$, is unity for the gas phase which implies that the Schmidt and Prandtl numbers are equal. Here, the Schmidt and Prandtl numbers are both set equal to one. This assumption also implies that the thermal and mass diffusivities are equal.

6. The value of $\rho\mathcal{D}_{im} = \rho\mathcal{D}$, the density times mass diffusivity, is the same for all gaseous species.

7. The gas and liquid mixtures behave ideally.

Runge states in his thesis that assumptions 5 and 6 are not justified and are used for convenience. Using constant properties is not necessary to obtain a solution, but, it simplifies the calculations. These simplifications are taken into account by fitting parameters to experimental data as described next.

The more volatile fuel components will evaporate faster than the less volatile components. As the mixture evaporates, the less volatile components increase in concentration, changing the fuel properties. These changes will cause erroneous results from a calculation of multiple component evaporation using constant properties that are the same for all species. Runge et al. remedy this problem with a weighted empirical correlation of $\rho\mathcal{D}$ based on the percent volume of liquid remaining:

$$\rho\mathcal{D} = V_p\rho\mathcal{D}_{hi} + (1 - V_p)\rho\mathcal{D}_{lo}, \tag{2.46}$$

where V_p is the percent volume of liquid remaining, $\mathcal{D}_{hi}$ is the upper limit diffusivity constant, $\mathcal{D}_{lo}$ is the lower limit diffusivity constant. These constants are determined

through empirical parameter fitting to experimental data. Time is then scaled by $\rho\mathcal{D}/\rho\mathcal{D}_r$, where the subscript r denotes a constant reference value, to correct for the changes in the actual $\rho\mathcal{D}$ product.

The descriptions presented in Runge's thesis (17) and the article (16) report different values for the parameters $\mathcal{D}_{hi}$ and $\mathcal{D}_{lo}$. Reference (16) obtains the best-fit parameters shown in table 2.1. However, reference (17) reports that the best fit occurs when the values are those found in table 2.2.

Fuel	$\mathcal{D}_{lo} * 10^5, cm^2/s$	$\mathcal{D}_{hi} * 10^5, cm^2/s$
JP-4	2.0	4.0
JP-8	2.0	11.0

Table 2.1 $\rho\mathcal{D}$ coefficients reported in the article.

Fuel	$\mathcal{D}_{lo} * 10^5, cm^2/s$	$\mathcal{D}_{hi} * 10^5, cm^2/s$
JP-4	2.0	7.0
JP-8	4.0	14.0

Table 2.2 $\rho\mathcal{D}$ coefficients used in Runge's thesis.

2.3.3.2   Equations.   We begin with equation (2.8) in section 2.2, Fick's first law of diffusion:

$$\mathbf{n}_A = \rho_A \mathbf{v}_A = Y_A(\mathbf{n}_A + \mathbf{n}_B) - \rho\mathcal{D}_{AB}\nabla Y_A$$

If we assume spherical symmetry, then this becomes a one-dimensional problem and the flux of A is given by:

$$n_A = Y_A(n_A + n_B) - \rho\mathcal{D}_{AB}\frac{dY_A}{dr} \tag{2.47}$$

For multicomponent mixtures, an effective binary diffusivity $\mathcal{D}_{im}$ for the diffusion of i in a mixture of N species can be defined by an analogous equation as in

Bird et al. (1):

$$n_i = Y_i \sum_{k=1}^{N} n_k - \rho \mathcal{D}_{im} \frac{dY_i}{dr} \qquad (2.48)$$

where the subscript m denotes the rest of the mixture. Multiplying both sides of equation (2.48) by $4\pi r^2$ results in an expression for the mass of species i leaving the total area of a sphere of radius r, M_i:

$$M_i = Y_i \sum_{k=1}^{N} M_k - 4\pi r^2 \rho \mathcal{D}_{im} \frac{dY_i}{dr}$$

Then, dividing both sides by $4\pi r_0 \rho \mathcal{D}_{im}$ yields equation (1) of Law:

$$\mathcal{M}_i = Y_i \sum_{k=1}^{N} \mathcal{M}_k - R^2 \frac{dY_i}{dR} \qquad (2.49)$$

where $\mathcal{M} = M/(4\pi r_0 \rho \mathcal{D}_{im})$ is the non-dimensional mass evaporation rate and $R = r/r_0$.

The equations for the changes in radius, mass, and temperature are all based upon the normalized aggregate vaporization rate, $\mathcal{M}_F = \sum_{i=1}^{N} \mathcal{M}_i$, as will be described in section 2.3.3.2.

The energy equation used by Law (9) can be arrived at from the more familiar form of the energy equation (see equation (6-105) of Kuo (8)):

$$r^2 \rho v \frac{dc_p T}{dr} = \frac{d}{dr}(r^2 \frac{\lambda}{c_p} \frac{dc_p T}{dr}) + r^2 \dot{Q} \qquad (2.50)$$

where λ is the thermal conductivity, and $\dot{Q}$ is the heat of reaction per unit mass of fuel during combustion. For pure evaporation (no combustion), $\dot{Q}$ is zero. Following the analysis presented by Kuo, and then non-dimensionalizing the variables, we arrive at equation (2) of Law:

$$\mathcal{M}_F(\mathcal{T} - \mathcal{T}_s) - R^2 \frac{d\mathcal{T}}{dR} = -\mathcal{M}_F(\mathcal{L} + H) \qquad (2.51)$$

2-26

where $\mathcal{T} = Tc_p/L_r$, c_p is the constant gas specific heat, L_r is a reference latent heat of vaporization, and $\mathcal{L} = \sum_{i=1}^{N} \epsilon_i L_i/L_r$ is the species weighted, non-dimensional latent heat of vaporization. The heat input function, H, is the difference between the heat transferred to the droplet and that needed for vaporization. It is not explicitly defined and is obtained, along with equations (2.52),(2.55), and (2.57), by solving equations (2.49) and (2.51).

The equation of change for the non-dimensional mass of species i is given in reference (17) by:

$$\frac{dm_i}{dt} = -\mathcal{M}_i R \quad i = 1..N, \tag{2.52}$$

where $\mathcal{M}_i = \epsilon \mathcal{M}$ is the spherically symmetric mass vaporization rate and $R = r/r_0$ is the non-dimensional radius with r being the radius at time t and r_0 the initial radius of the droplet. The spherically symmetric mass vaporization rate, $\mathcal{M}$, is given as in Law (9):

$$\mathcal{M} = ln(1 + B) \tag{2.53}$$

where

$$B = \frac{Y_F}{1 - Y_F} \tag{2.54}$$

is the driving force for evaporation, the mass transfer or Spalding number. In calculating $\mathcal{M}_i$, $\epsilon_i = Y_i/Y_F$ is the ratio of the mass fraction of i in the vapor phase at the surface of the droplet, taking into account the presence of air, to the sum of those mass fractions, Y_F.

The vaporization rate is empirically adjusted for convective effects using the Sherwood number, which is computed using equation (2.19) of section 2.2:

$$N_S = 2.0 + 0.6 N_R^{1/2} N_c^{1/3}$$

where the Schmidt number has been set equal to one. Notice that since it has been assumed that $N_c = N_P$, the Sherwood number is the same as the Nusselt number

for heat transfer. As we will see next, $\mathcal{M}$ is also used in the calculation of the heat transfer.

The equation for the change in temperature with respect to time is:

$$\frac{d\mathcal{T}}{dt} = \frac{H\mathcal{M}}{\rho_\ell R^2} \qquad (2.55)$$

where H is the heat input function, $\mathcal{M}$ is the spherically symmetry mass vaporization rate of the droplet, and ρ_ℓ is the density of the liquid fuel.

The heat input function is calculated by

$$H = (1 - Y_F)(\mathcal{T}_\infty - \mathcal{T}_s)/Y_F - \mathcal{L}, \qquad (2.56)$$

where $\mathcal{T}_\infty = T_\infty c_p/L_r$ is the non-dimensional ambient temperature, $\mathcal{T}_s = T_d c_p/L_r$ is the non-dimensional droplet temperature, c_p is the gas phase specific heat at the surface of the droplet, $\mathcal{L} = \sum_{i=1}^{n} L_i/L_r$ is the latent heat of vaporization, L_i is the latent heat of species i, and L_r is a reference latent heat.

The equation for the change in non-dimensional radius is given by:

$$\frac{dR}{dt} = \frac{-\mathcal{M}}{3R\varrho} \qquad (2.57)$$

where $\varrho = \rho_\ell/\rho_r$ is the liquid density divided by a reference density. If this equation is multiplied by $3R^2\varrho$, then we obtain:

$$3R^2\varrho\frac{dR}{dt} = \frac{d}{dt}\varrho R^3 = -\mathcal{M}R$$

since ϱ is assumed to be constant. This final form is the equation implemented in Runge's code that is listed in the appendix of his thesis. Runge then updates $R^3\varrho$ and recovers R from this value.

The equations presented in the article by Runge et. al (16), where most of the experimental data in chapter III appears, are different from those found in Runge's thesis (17). The non-dimensional spherically symmetric mass vaporization rate is given in reference (16) by:

$$\mathcal{M} = R\rho\mathcal{D}ln(1+B) \tag{2.58}$$

This rate is then corrected to account for convective effects by multiplying by the Sherwood number, which is given by:

$$N_S = (2.0 + 0.6N_R^{1/2}N_c^{1/3})(1 + \frac{1}{1-Y})^{-0.7}$$

In the case of heat transfer, it is corrected for convective effects by multiplying by the Nusselt number, which is given by:

$$N_u = (2 + 0.6N_R^{1/2}N_P^{1/3})(1 + \mathcal{T}_\infty - \mathcal{T}_s)^{-0.7}$$

The time rate of change of non-dimensional radius, R, temperature, $\mathcal{T}_s$, and mass, m, is then given by:

$$\frac{dR}{dt} = -\frac{\mathcal{M}}{3R\varrho} \tag{2.59}$$

$$\frac{dm_i}{dt} = -\epsilon_i\mathcal{M} \tag{2.60}$$

$$\frac{d\mathcal{T}_s}{dt} = \frac{c_p H\mathcal{M}}{c_\ell R^3 \varrho} \tag{2.61}$$

where c_ℓ is the liquid specific heat of the mixture. The heat input function, H is given by:

$$H = Q\frac{N_u}{2} - \mathcal{L}\frac{N_s}{2} \tag{2.62}$$

where $\mathcal{L}$ is given as in reference (17), and Q is given by:

$$Q = \frac{\mathcal{T}_\infty - \mathcal{T}_s}{B}$$

2-29

Unfortunately, we were not able to use the equations presented in reference (16) to reproduce exactly the predictions presented in that paper. This will be further discussed in chapter III.

III. Comparison of the Droplet Evaporation Calculations

3.1 Overview

In this chapter, evaporation calculations of Clewell (3), Runge et al. (16), and Runge's thesis (17) are compared. Clewell's algorithm was chosen because it is more advanced than Lowell's and the contribution by Pfeiffer et al. was improvement to the dispersion calculations which are not considered here. The evaporation algorithms of Clewell and Pfeiffer should predict almost identical results and a short comparison of the predictions is performed to verify that this is the case.

3.2 Comparison of the Predictions of Clewell and Pfeiffer

Pfeiffer's algorithm was available in electronic format as part of his thesis at AFIT (12). Clewell's algorithm was implemented from the code listing found in reference (3).

The models of Clewell and Pfeiffer should be almost identical with respect to evaporation because Pfeiffer used the model of Clewell to predict evaporation rates, focusing instead on improving the dispersion model. Figure 3.1 compares the predictions of the evaporation of JP-4. The initial temperature was calculated from an aircraft velocity of 175 m/s, the ground temperature was 273.15 K, the initial diameter was 500 μm, and the jettison altitude was 1500.0 m. Notice from figure 3.1 that there is difference in the diameter predictions of Clewell and Pfeiffer.

The major reason is the difference in the temperatures predicted. Clewell's algorithm predicts a large decrease in temperature initially. This is due to evaporative cooling and Pfeiffer's predictions should be, at least qualitatively, exhibiting this same behavior. Although the two algorithms are supposed to be the same, the temperature predicted by Pfeiffer does not match the prediction of Clewell's algorithm, as shown in figure 3.2. This would explain why Clewell's algorithm predicts a different diameter than Pfeiffer's algorithm. Pfeiffer's temperature prediction is
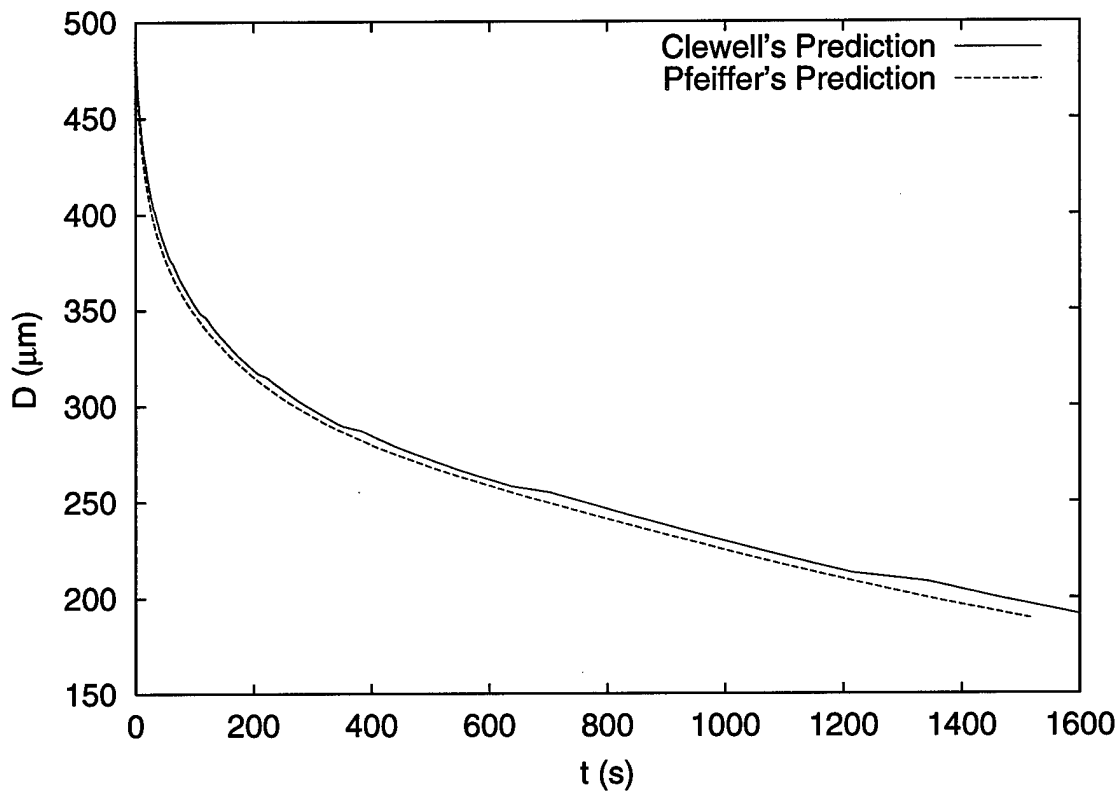
Figure 3.1   Comparison of Clewell's and Pfeiffer's predictions of JP-4 droplet diameter versus time during evaporation. Jettison velocity $= 175m/s$, $T_\infty = 0^o$ C at the ground, $D_0 = 500$ μm, jettison altitude $= 1500$ m.

initially higher than Clewell's, leading to more evaporation and a smaller droplet diameter as shown in figure 3.1.

In the version of Pfeiffer's algorithm that was provided with the AFIT thesis, the calculation of the steady state temperature is erroneous. The calculation of Q and Q' for the Newton-Raphson iterative method had to be corrected. Furthermore, the droplet temperature was not being updated after the steady-state temperature was calculated as indicated by the short intervals where the predicted temperature does not change in figure 3.2. Thirdly, the algorithm only computed the droplet cooling at the first time step and then switched to strictly computing the steady state temperature. The initial calculation of the number of moles of fuel also had to be corrected. Once the corrections were made, Pfeiffer's prediction of the droplet
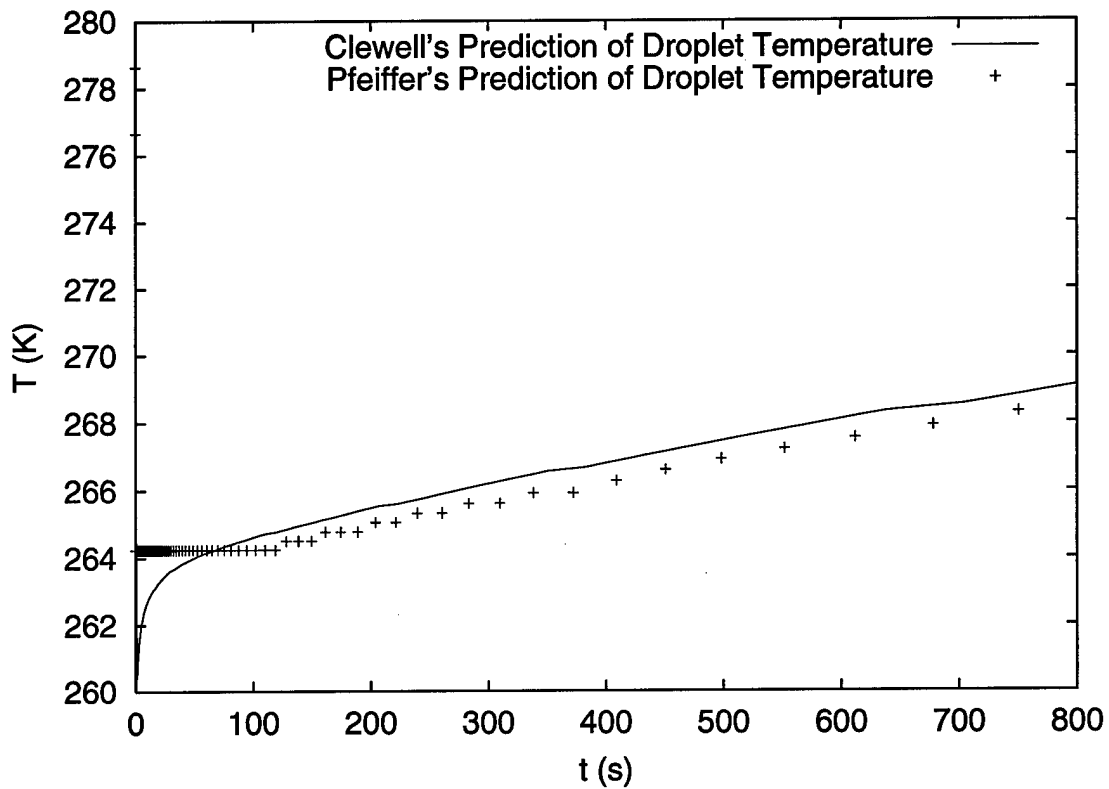
Figure 3.2   Comparison of Clewell's and Pfeiffer's calculations of JP-4 droplet temperature versus time showing the error in Pfeiffer's calculation of temperature. Jettison velocity $= 175m/s$, $T_\infty = 0^o\ C$ at the ground, $D_0 = 500\ \mu m$, jettison altitude $= 1500\ m$.

temperature is smooth and more closely matching that of Clewell. Pfeiffer's corrected and uncorrected droplet temperature predictions are compared to Clewell's in figure 3.3. Notice that after the corrections are made, the prediction's of Pfeiffer and Clewell are almost identical. The remaining difference in the initial temperature decrease is due to differences in the time step adjustment which is explained below.

The predictions of Clewell and Pfeiffer are still not exactly the same. This may be because Pfeiffer uses a different approach to adjusting the time step. If the mass evaporated during any time step is greater than some predefined maximum, which is nominally 1% of the initial droplet mass, Clewell simply halves the computed changes in time, altitude, and mass until the amount of mass evaporated is below
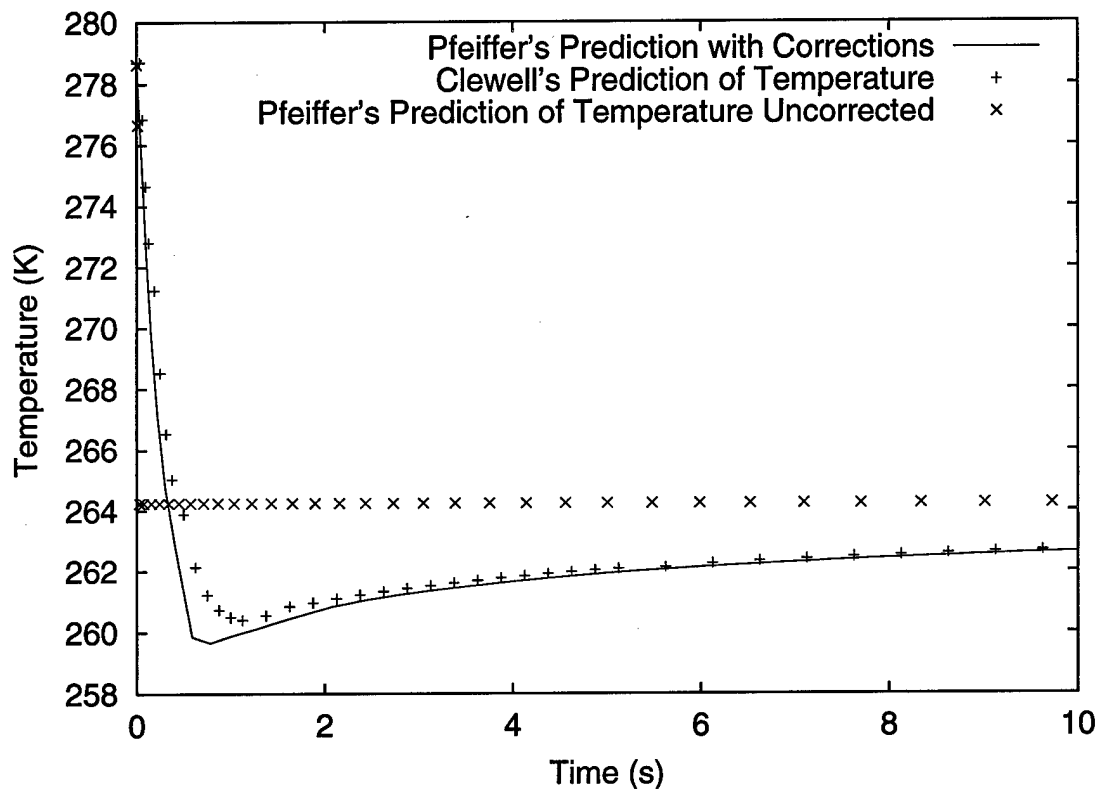
Figure 3.3   Comparison of Pfeiffer's corrected and uncorrected calculations of JP-4 droplet temperature versus time to those of Clewell showing the error in Pfeiffer's original calculation of temperature. Jettison velocity = $175 m/s$, $T_\infty = 0^o\ C$ at the ground, $D_0 = 500\ \mu m$, jettison altitude = $1500\ m$.

the defined maximum amount. Also, the temperature change is not halved if the steady-state temperature is calculated and results in a droplet temperature that is closer to the ambient temperature than it was on the previous time step. Pfeiffer calculates the factor needed to reduce the change in mass evaporated to the maximum amount allowed and then scales the changes in mass, altitude, temperature, and time uniformly rather than just halving the changes. Furthermore, Pfeiffer scales the change in temperature regardless of the result of the temperature change. Pfeiffer's method is more efficient because Clewell's method may require more than one scaling iteration and may reduce the changes in mass, temperature, and altitude by more than is necessary. Figure 3.4 is a comparison of Clewell's prediction of JP-4 droplet

temperature, using Pfeiffer's method of scaling the changes, to that of Pfeiffer with the errors corrected. The time scale has again been shortened to the first 10 seconds of the simulation in order to observe the point where the largest discrepancy between the two models' predictions occurred. Notice that Clewell's prediction is much closer to Pfeiffer's now that Pfeiffer's scaling method is used by both models.
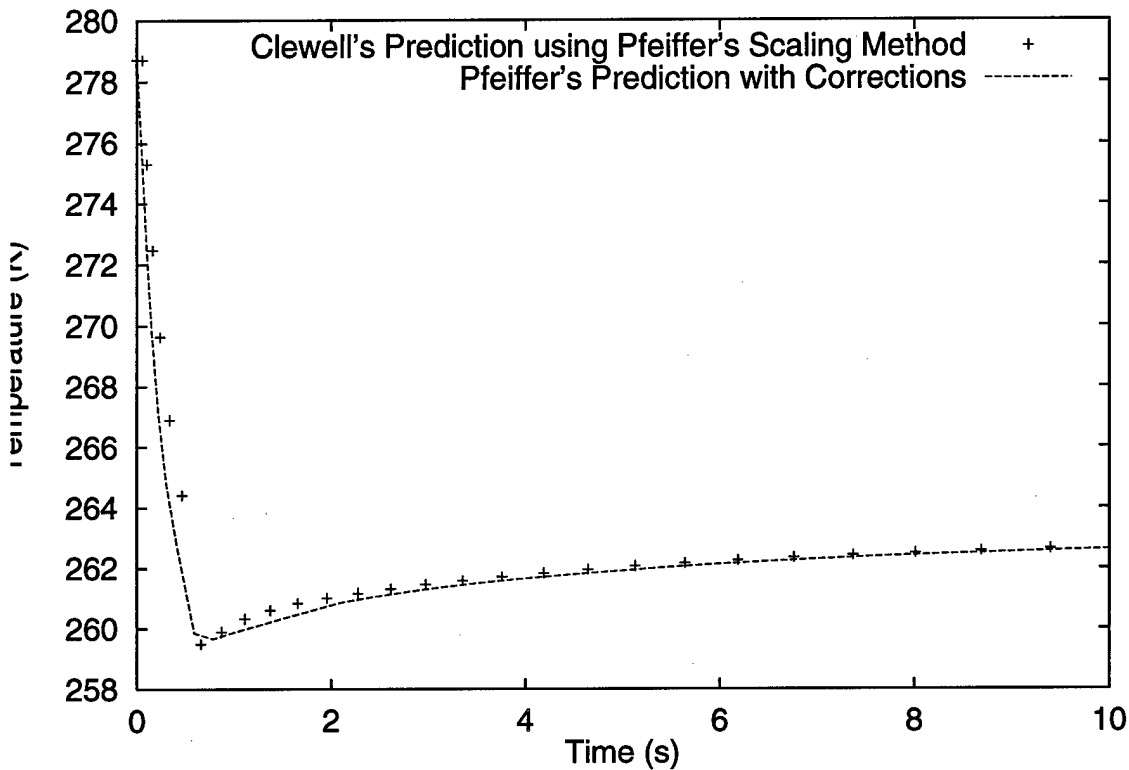
Figure 3.4   Comparison of Pfeiffer's corrected calculations and Clewell's calculations of droplet temperature versus time using Pfeiffer's method of scaling. Jettison velocity $= 175 m/s$, $T_\infty = 0^o$ C at the ground, $D_0 = 500$ μm, jettison altitude $= 1500$ m.

The corrected droplet diameter predictions and uncorrected predictions of Pfeiffer are compared to Clewell predictions of droplet diameter using Pfeiffer's method of scaling in figure 3.5. The time scale has been shortened to the first 200 seconds of the simulation, where the temperature difference was the largest. Pfeiffer's corrected temperature calculation led to a lower temperature at small time which

leads to a larger droplet diameter. After Pfeiffer's code is corrected and Clewell's code is modified to adjust the changes as Pfeiffer does, the predictions are closer.
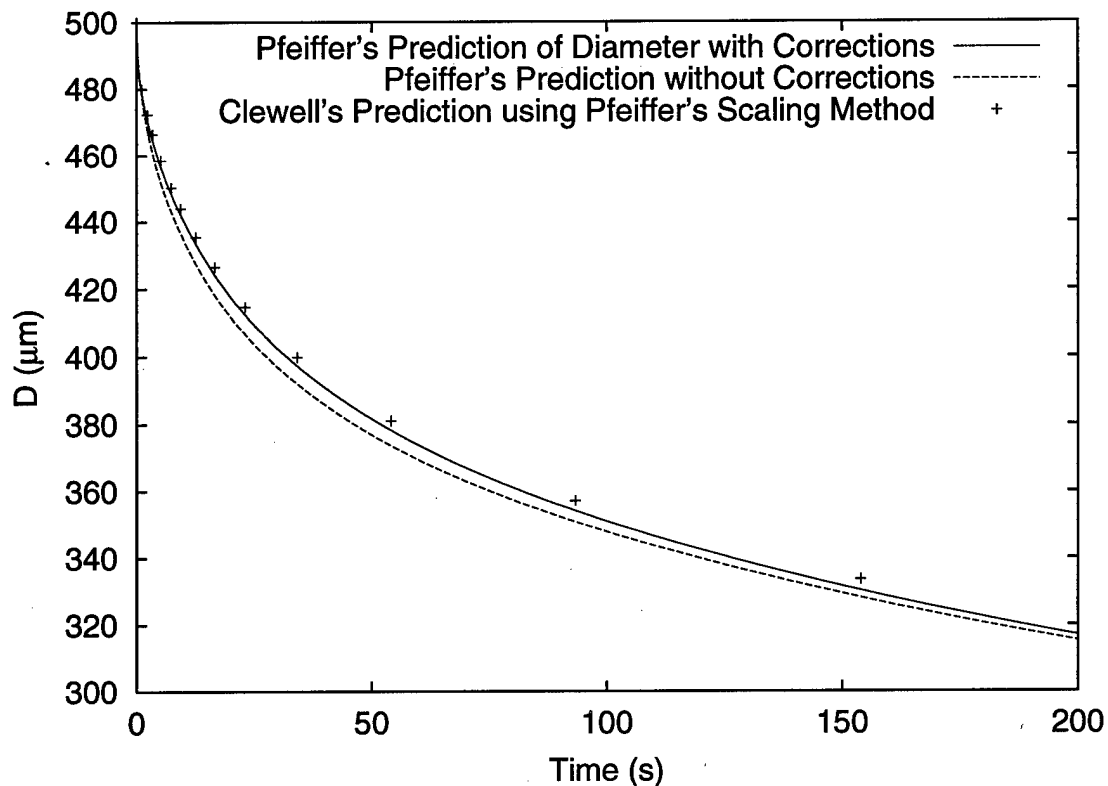
Figure 3.5   Comparison of Pfeiffer's uncorrected and corrected calculations of droplet diameter versus time to Clewell's calculation using Pfeiffer's method of scaling. Jettison velocity $= 175 m/s$, $T_\infty = 0^o$ C at the ground, $D_0 = 500$ μm, jettison altitude $= 1500$ m.

3.3   Comparison of Clewell and Runge, Teske, Polymeropolous

For comparison to experimental data found in (16), where the droplets were suspended in a chamber from thin thermocouple wires in a uniform stream of dry air, Clewell's algorithm was modified to match the experimental conditions. The algorithm originally computed the change in droplet altitude, the initial droplet temperature was based on the jettison velocity, and the Reynolds number was computed using the droplets terminal velocity at its current size. For comparison to the exper-

3-6

imental measurements, the altitude is fixed at 0 m to simulate droplet suspension and the Reynolds number is calculated using a fixed air velocity. The initial droplet temperature was set equal to the ambient temperature instead of being calculated.

Figure 3.6 compares the measurements of heptane evaporation taken by Runge with the predictions shown in Runge's thesis (17) and Clewell predictions. The initial conditions are reported in Table 3.1. For this single component fuel, the $\rho\mathcal{D}$ product was assumed by Runge to be constant and was computed to be 8.5 x 10^{-5} g/(cm s) by using the Fuller correlation as recommended by Reid et al. (15). The Fuller correlation was also used to compute the diffusivity for Clewell's prediction as well. For both predictions, the Lee-Kessler relation and Pitzer correlation were used for the calculation of the vapor pressure and latent heat of vaporization, respectively (15). The boiling point, molecular weight, and density of heptane were taken from the data corresponding to C7-paraffins in the table presented in the appendix of reference (12).

Constants	Values
$D_0(\mu m)$	638
$T_\infty(^oC)$	20
$v(m/s)$	2
$\rho\mathcal{D}(g/cm/s)$	$8.5\mathrm{x}10^{-5}$

Table 3.1   Initial conditions for evaporation of heptane.

Figure 3.6 shows that the predictions of Runge are almost an exact match to the measured data, and that Clewell's predictions are reasonably close. This is not surprising since the Runge's algorithm was developed by fitting the free $\rho\mathcal{D}$ parameter to JP-4 and JP-8 evaporation data and heptane behaves similarly.

The remaining predictions and measurements of evaporation that appear in Runge's thesis cannot be compared because the initial diameters of the droplets are not reported. Runge states that this does not need to be considered because the data is normalized to take into account the initial droplet size. However, this is not the
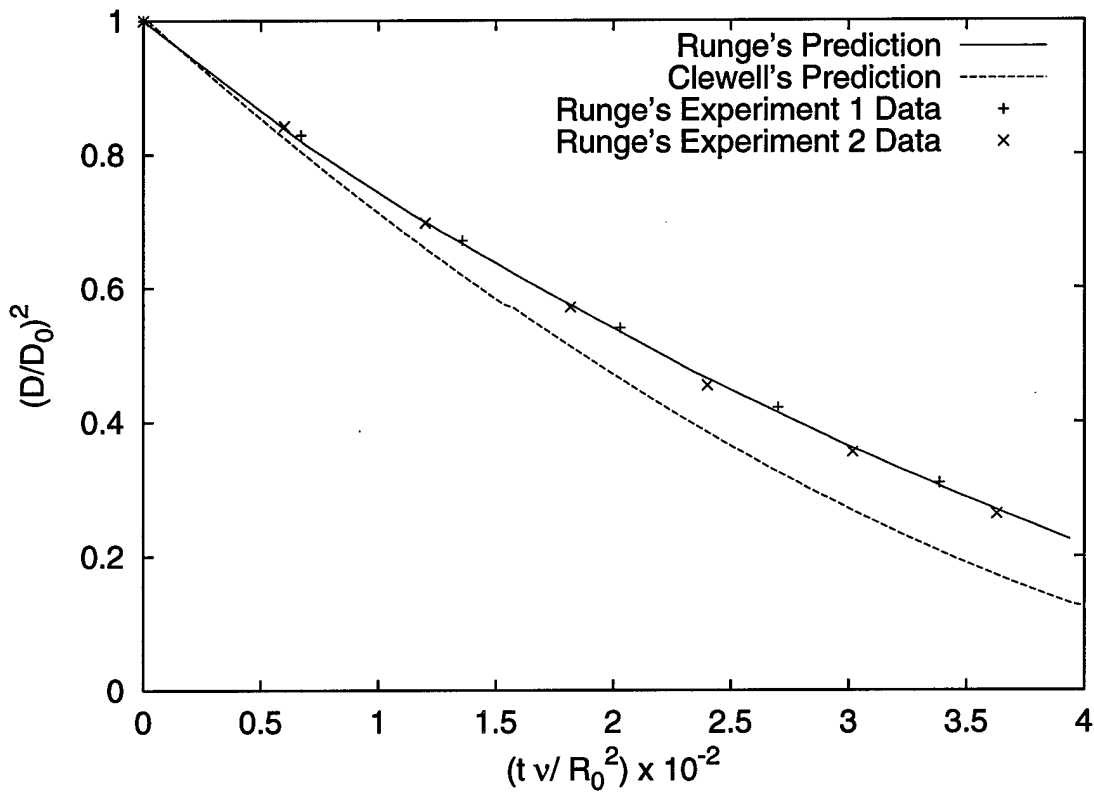
Figure 3.6   Predictions of Heptane evaporation compared to experimental data. Runge's prediction and the experimental data were taken from Runge's thesis and Clewell's prediction was generated using Clewell's algorithm. $D_0 = 638\mu m$, $T_\infty = 20^o\ C$, $u = 2m/s$

case unless a common reference Reynolds number is used for all calculations because the droplet diameter is also needed to compute the Reynolds number.

Unfortunately, the calculations presented in reference (16) could not be reproduced from the equations in the appendix of reference (16). Recall the spherically symmetric mass vaporization rate, $\mathcal{M}$, without corrections for convective effects, as given by reference (16):

$$\mathcal{M} = \frac{N_S}{2} R\ \rho D\ ln(1 + B)$$

The question is, what is ρD? There is no ρ or D listed in the nomenclature table of reference (16). If we follow the notation used for R, then $D = D'/D'_0$ and

$\rho = \rho'_\ell / \rho'_r$ where the primes denote dimensional variables. This interpretation does not reproduce the predictions though. Alternatively, ρD could be a reduced mass diffusivity-density product, $(\rho' \mathcal{D}')/(\rho' \mathcal{D}')_r$, since the variables in question are not primed which suggests that they have been divided by a reference value. However, this approach leads to a dependence on the value of $(\rho' \mathcal{D}')_r$, and this value is not specified. Many different permutations of what the variables could be were tried and none led to predictions similar to the ones presented in the figures of the article. Due to these difficulties with the equations presented in the article (16), the curves presented in the figures are used rather than reproducing them using the equations.

Figure 3.7   Comparison of the predictions of Clewell, Runge's thesis, and Runge et al. to the experimentally measured non-dimensional surface area of a JP-4 droplet versus non-dimensional time. Ambient air velocity = 3 m/s, $T_\infty = 21^\circ$ C, $D_0 = 636\ \mu m$.

Figures 3.7 through 3.14 are comparisons of the calculations performed using the equations of Clewell, Runge's thesis, and the Runge et al. article to experimental data measured by Runge et al. The non-dimensional time is computed as $10^{-2}\ t\nu/r_0^2$ where ν is the kinematic viscosity of air. The non-dimensional surface area is computed as $(D/D_0)^2$. The ambient air flow is denoted by u, the ambient temperature is denoted by T_∞, and the initial droplet diameter is denoted by D_0.

Notice that the equations used in the thesis by Runge (17) produce results that are very close to those presented in the article. Although the formulations are not the same, both sets of equations are based on the approach of Law and we would expect that the calculations would be similar.

Figure 3.8   Comparison of the predictions of Clewell, Runge's thesis, and Runge et al. to the experimentally measured non-dimensional surface area of a JP-4 droplet versus non-dimensional time. Ambient air velocity = 3 m/s, $T_\infty = -15^o$ C, $D_0 = 600\ \mu m$.
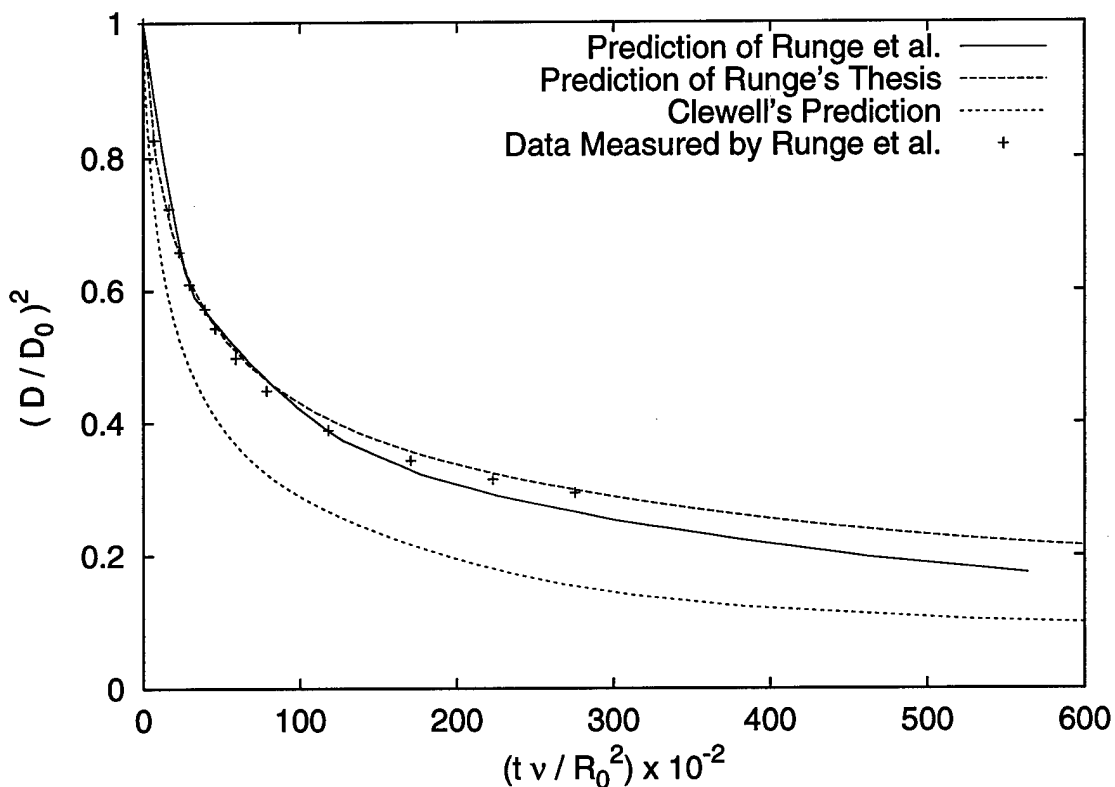
Figure 3.9   Comparison of the predictions of Clewell, Runge's thesis, and Runge et al. to the experimentally measured non-dimensional surface area of a JP-8 droplet versus non-dimensional time. Ambient air velocity = 3 m/s, $T_\infty = -14.5^\circ$ C, $D_0 = 645$ μm.

With the exception of figure 3.9, Clewell predicts a smaller droplet surface area than was measured and calculated by the other approach. The main difference between the two approaches is the calculation of the gas phase diffusivity and mass density of the fuel components.

Clewell computes the diffusivity of each species in air using an empirical correlation that is derived from one found in Bird et al. (1) using parameters that are typical of hydrocarbons. Clewell handles the calculation of the mass density as in section 2.2. Recall that the gas phase mass density is combined with the mass fraction of species i to yield the gas phase mass density of species i. The mass density

of species i can then be computed by:

$$\rho_i = c\chi_i w_i$$

The approach of Runge and Runge et al. requires that the coefficients used to calculate the mass density times diffusivity product, $(\rho\mathcal{D})$, be determined through fitting curves to the experimental data. A reference value, $(\rho\mathcal{D})_r$, is used for the product in the calculations of the rates of change. Then the dimensional time is scaled by the factor $(\rho\mathcal{D})_r/(\rho\mathcal{D})$ in order to match the experimental data.

This difference explains why the calculations of Clewell's algorithm appear to be more sensitive to temperature changes. Clewell computes the diffusivity as a function of temperature, but, Runge's algorithm uses the same $\rho\mathcal{D}$ product regardless of the temperature. This explains why Clewell predicts a larger JP-8 droplet surface area in figure 3.9, where the ambient temperature is -14.5^o C, and a smaller JP-8 droplet surface area at the higher ambient temperatures. The same effect for JP-4 evaporation is seen by comparing figure 3.7, where $T\infty = 21^o$ C, and figure 3.8, where $T\infty = -15^o$ C. The difference between the prediction of Clewell and the measured data in figure 3.8 is greater than in figure 3.7 because the diffusivity is much smaller at the lower temperature, which leads to a larger droplet surface area.

In each comparison of the measurements to the calculations, the approach of Runge et al. and Runge's thesis produces very accurate predictions of the non-dimensional surface area. This is to be expected since Runge et al. used experimental data to fit the parameters used in the calculation.

Clewell's approach was not adjusted to match the experimental data and does not produce results that are as accurate as the other algorithms that use a $\rho\mathcal{D}$ product that has been fit to experimental data. Although the number of comparisons to experimental data is small, Clewell's algorithm seems to produce more accurate predictions of JP-8 evaporation than JP-4 evaporation. This may be because JP-8
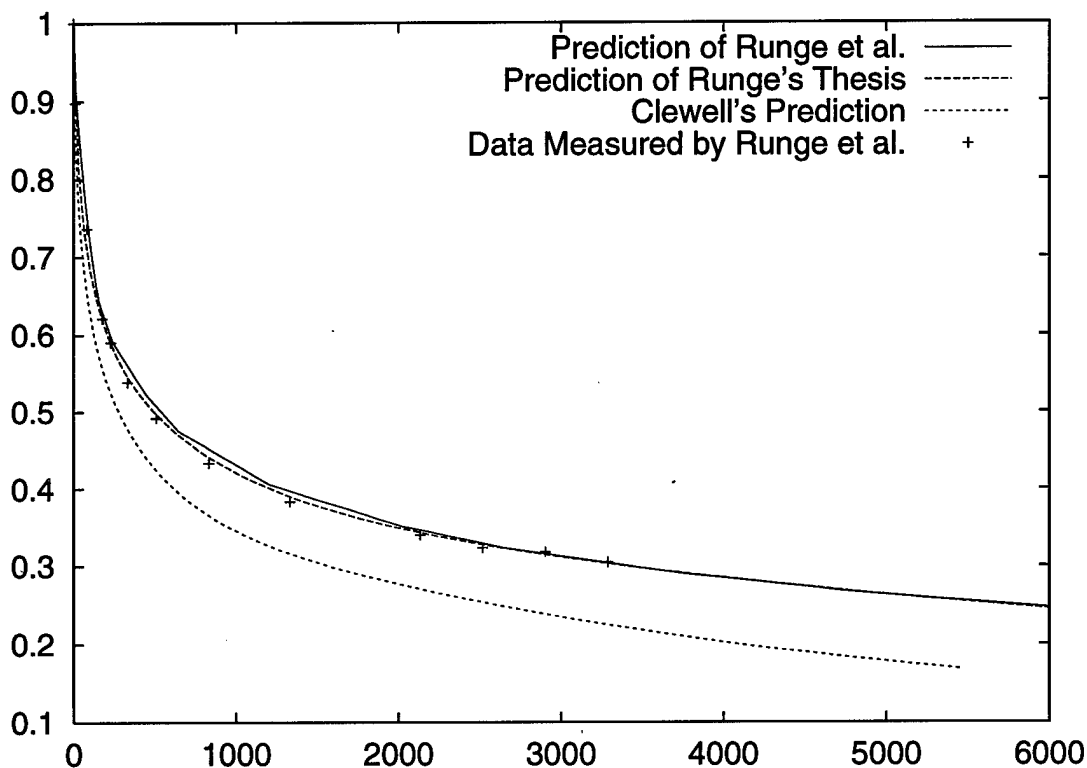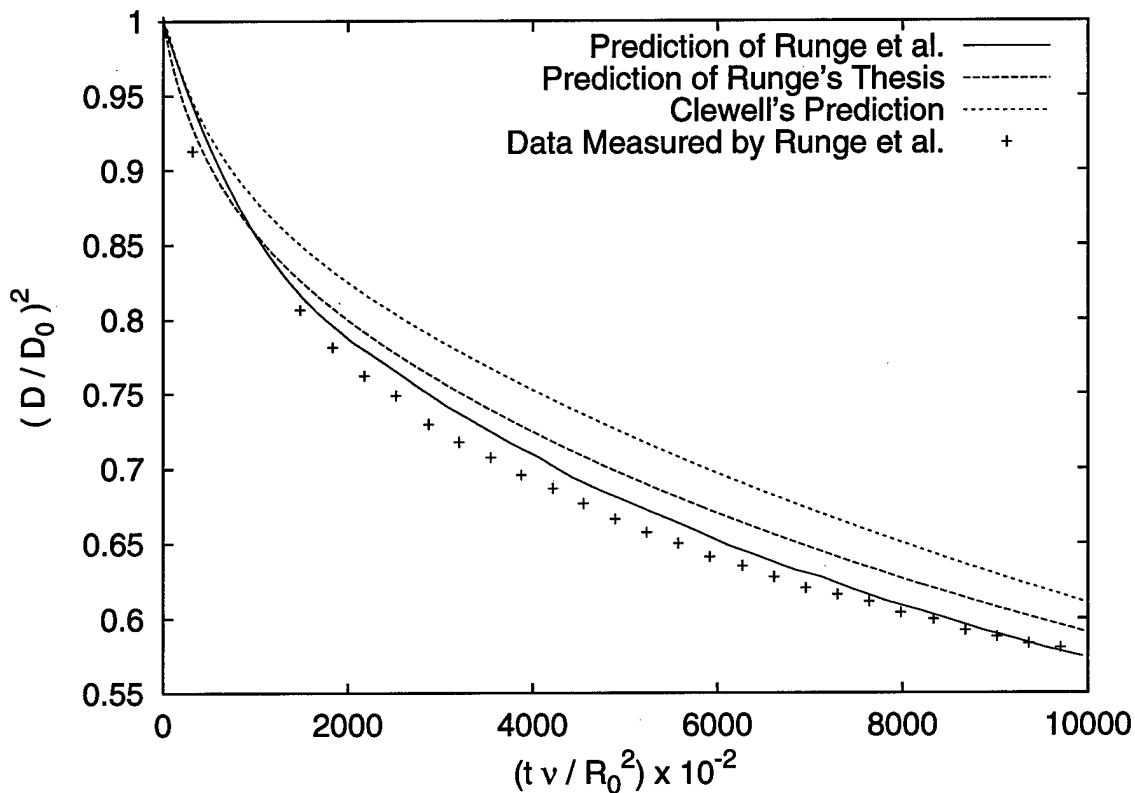
Figure 3.10   Comparison of the predictions of Clewell, Runge's thesis, and Runge et al. to the experimentally measured non-dimensional surface area of a JP-8 droplet versus non-dimensional time. Ambient air velocity = 3 m/s, $T_\infty = 21^o$ C, $D_0 = 636$ μm.

is less volatile than JP-4 and the JP-8 droplet temperature is not changed through evaporative cooling as much as the JP-4 droplet temperature (compare figures 3.13 and 3.14).

Figure 3.13 is a comparison of the predictions and experimental measurements of JP-8 droplet temperature during evaporation. The predictions of Clewell and Runge et. al appear to match fairly well and they are producing the same qualitative behavior as the measurements indicate. However, the experimental data shows a slower decrease in temperature than predicted by the models. This may be caused by the effects of suspending the droplets from a wire because the wire is being heated and cooled with the droplet. This increase the mass being cooled by the evaporative
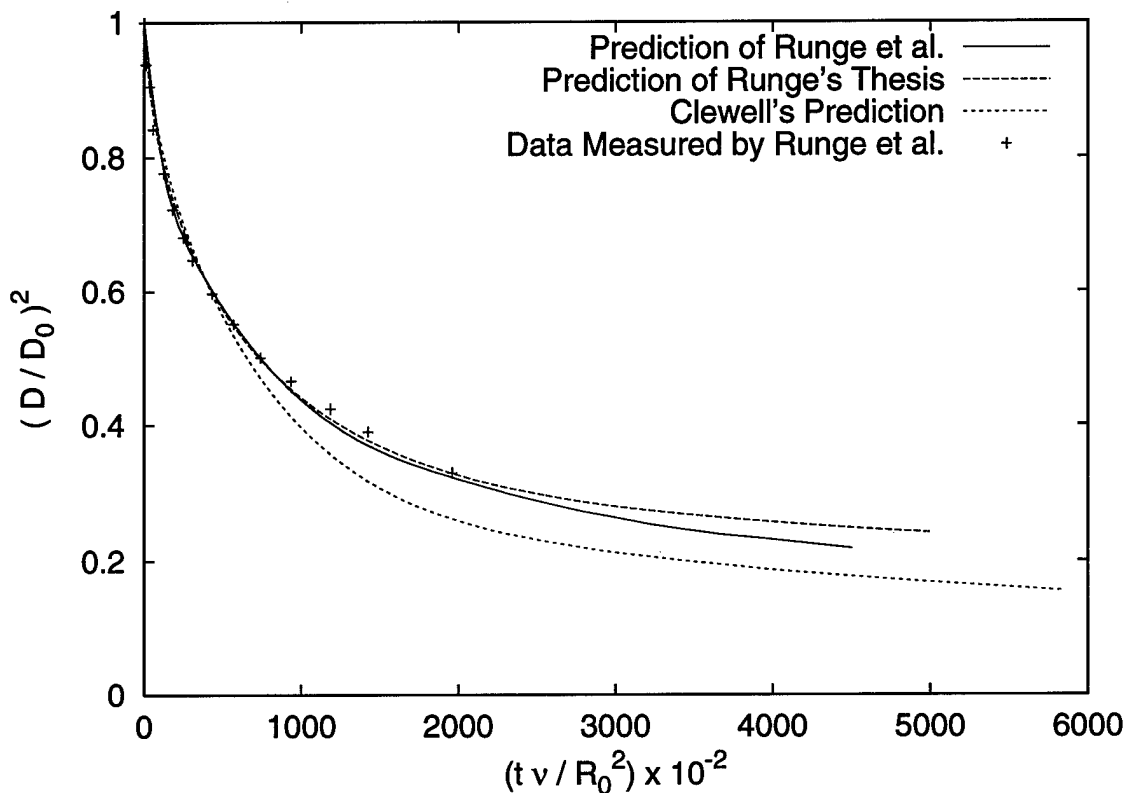
Figure 3.11   Comparison of the predictions of Clewell, Runge's thesis, and Runge et al. to the experimentally measured non-dimensional surface area of a JP-8 droplet versus non-dimensional time. Ambient air velocity = 1 m/s, $T_\infty = 10^o$ C, $D_0 = 647 \ \mu m$.

cooling and slow the process. The article of Runge et al. (16) examined the effect of the support wire on droplet evaporation measurements. The support wire alters the rate of heat transfer to the droplet and affects the droplet internal liquid motion. They performed a series of droplet evaporation measurements using different support materials and sizes until there was no apparent effect on the measured results. They concluded that a 25 μm diameter type K thermocouple support wire had negligible effects on the droplet evaporation. However, they did not specify whether they considered the effect on the droplet temperature. It appears as though the wire does affect the droplet temperature change while not significantly affecting the droplet diameter.
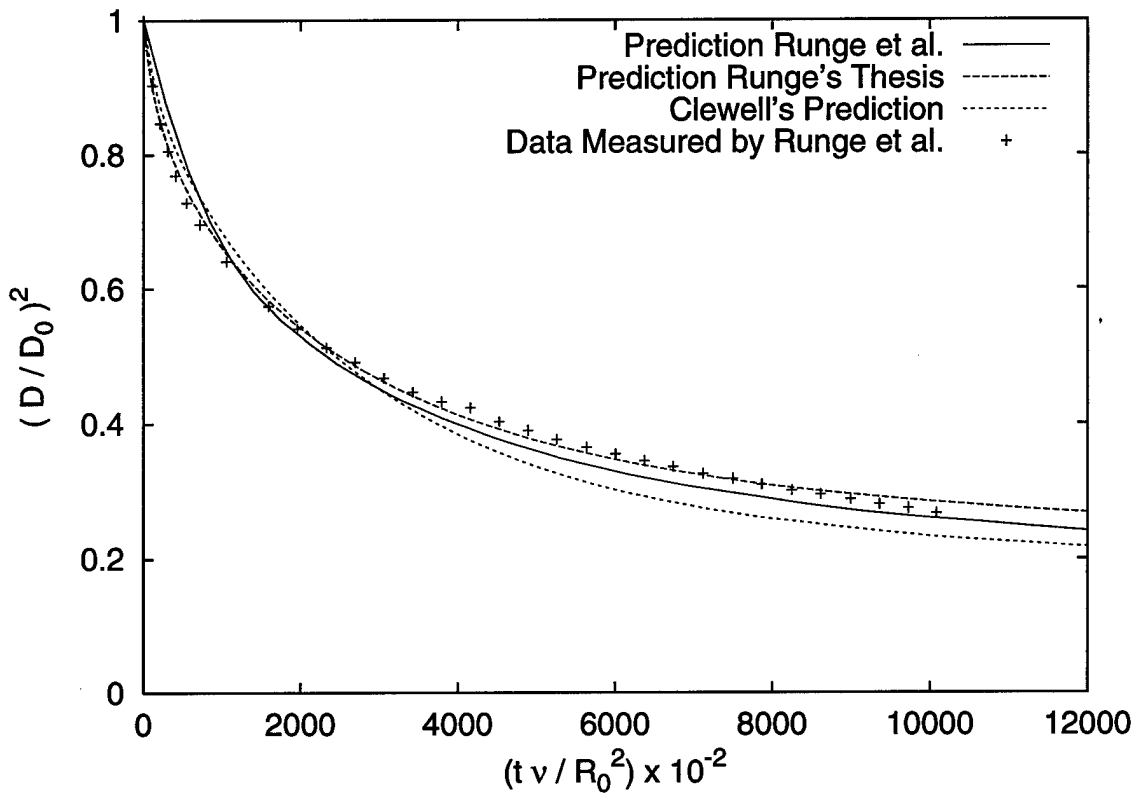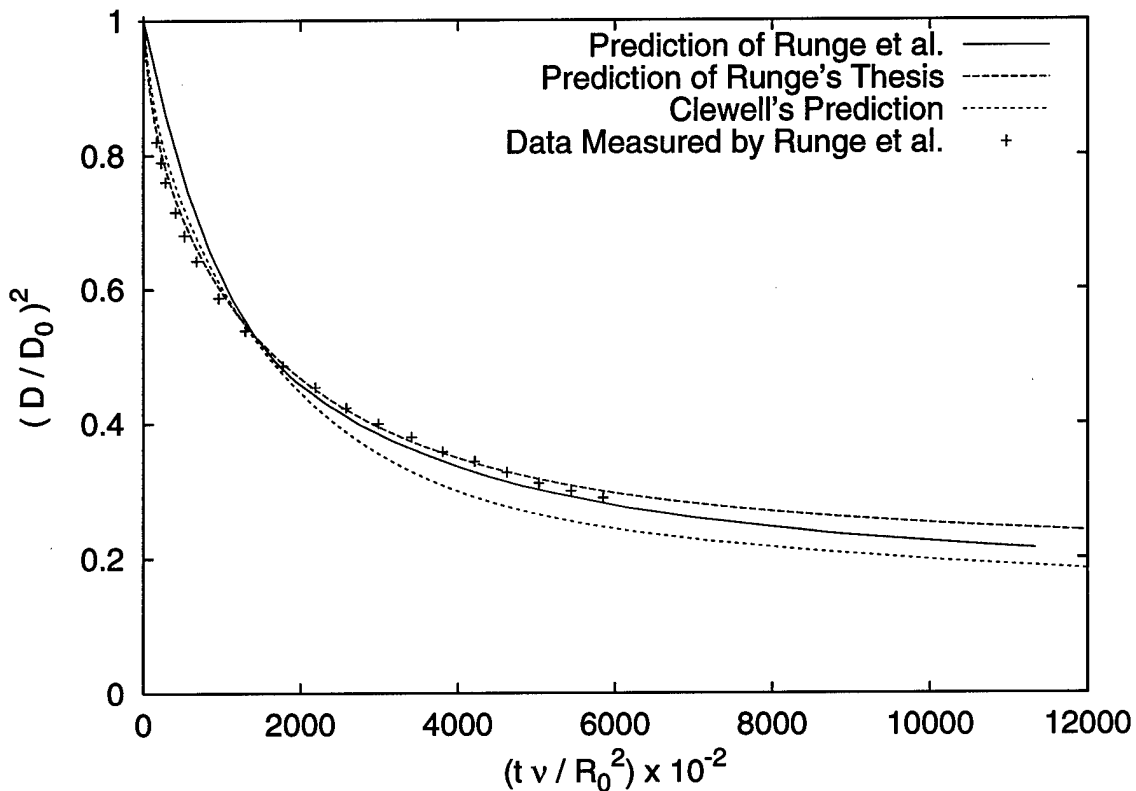
Figure 3.12 Comparison of the predictions of Clewell, Runge's thesis, and Runge et al. to the experimentally measured non-dimensional surface area of a JP-8 droplet versus non-dimensional time. Ambient air velocity $= 3$ m/s, $T_\infty = 10^o$ C, $D_0 = 639$ μm.

Notice that the scale of figure 3.13 is only 1.2 K. This is because JP-8 is less volatile than JP-4 and so the temperature is not affected by evaporative cooling as strongly. This means that although the temperature predictions for JP-8 are not exactly what was measured, the predictions are only wrong by a small amount.

Figure 3.14 is a comparison of the predictions and experimental measurements of JP-4 droplet temperature during evaporation. The initial temperature decrease predicted by the models occurs more quickly and is larger than the experimental measurement. It appears as though the support wire has again slowed and damped the initial decrease in temperature. Clewell's temperature calculations are closer to the measured values than the calculations of Runge et al.

3-15
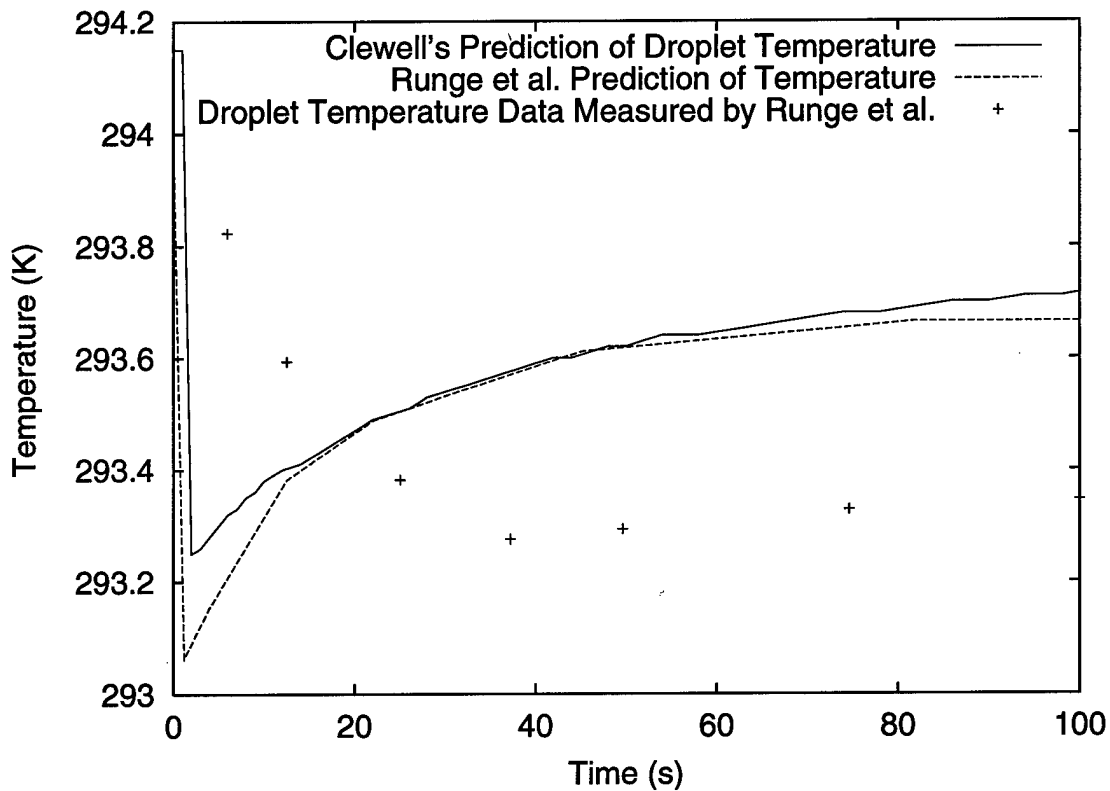
Figure 3.13   JP-8 droplet temperature predictions of Clewell and Runge et al. compared to measured JP-8 temperature during evaporation. $T_\infty = 0^o$ C, $D_0 = 639\mu m, u = 3m/s$.

Figures 3.15 through 3.18 are comparisons of the calculations of Clewell and Runge's thesis equations to experimental measurements of JP-4 droplet evaporation rates measured by the Arnold Engineering Development Center and presented in reference (4). In each case, the relationship between the calculations of the two approaches is the same. Clewell's algorithm calculates evaporation rates that are in agreement with than those calculated by Runge's thesis algorithm at a point in time between 20 and 30 seconds into the simulations. Before the time when the algorithms agree, Clewell's algorithm calculates higher evaporation rates than Runge's algorithm. At times beyond the point of agreement, Clewell's algorithm calculates lower evaporation rates than Runge's algorithm.

3-16
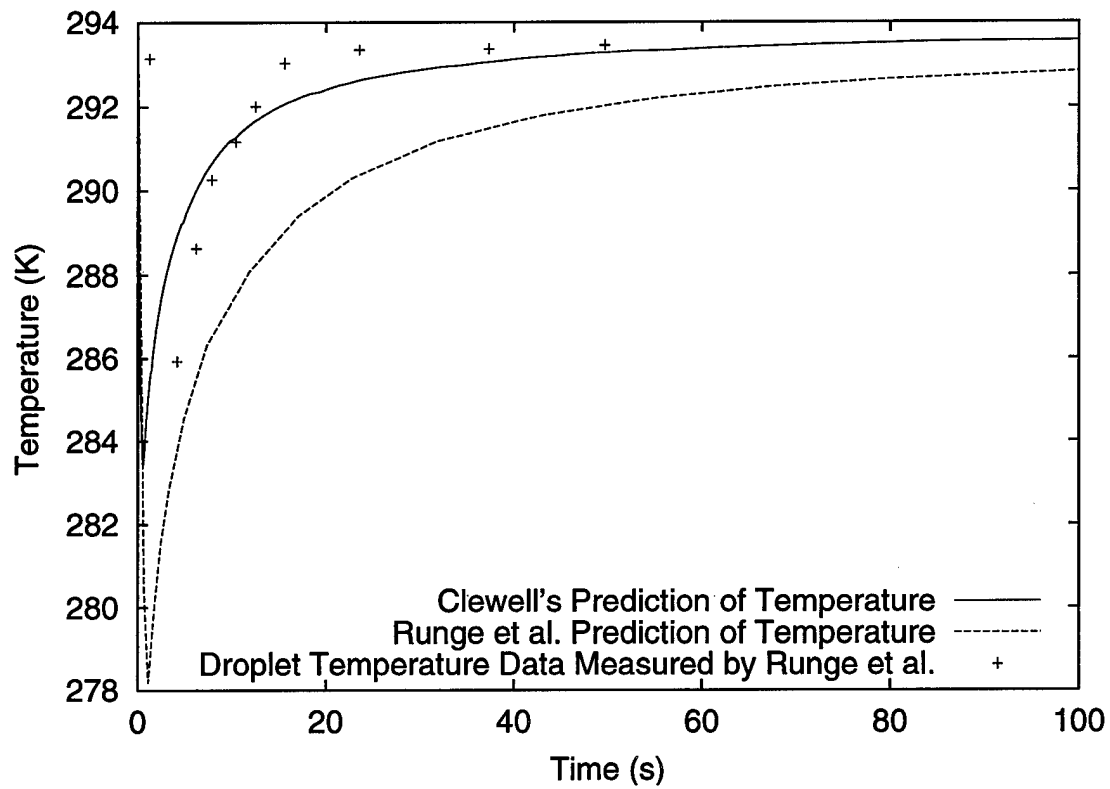
Figure 3.14 JP-4 droplet temperature predictions of Clewell and Runge et al. compared to measured JP-4 temperature during evaporation. $T_\infty = 0^o$ C, $D_0 = 646\mu m, u = 3m/s$.

Figure 3.15   Comparison of calculations of Clewell and Runge's thesis equations compared to measured JP-4 evaporation rate. $T_\infty = 20^o$ C, $D_0 = 1235\mu m, u = 3m/s$.
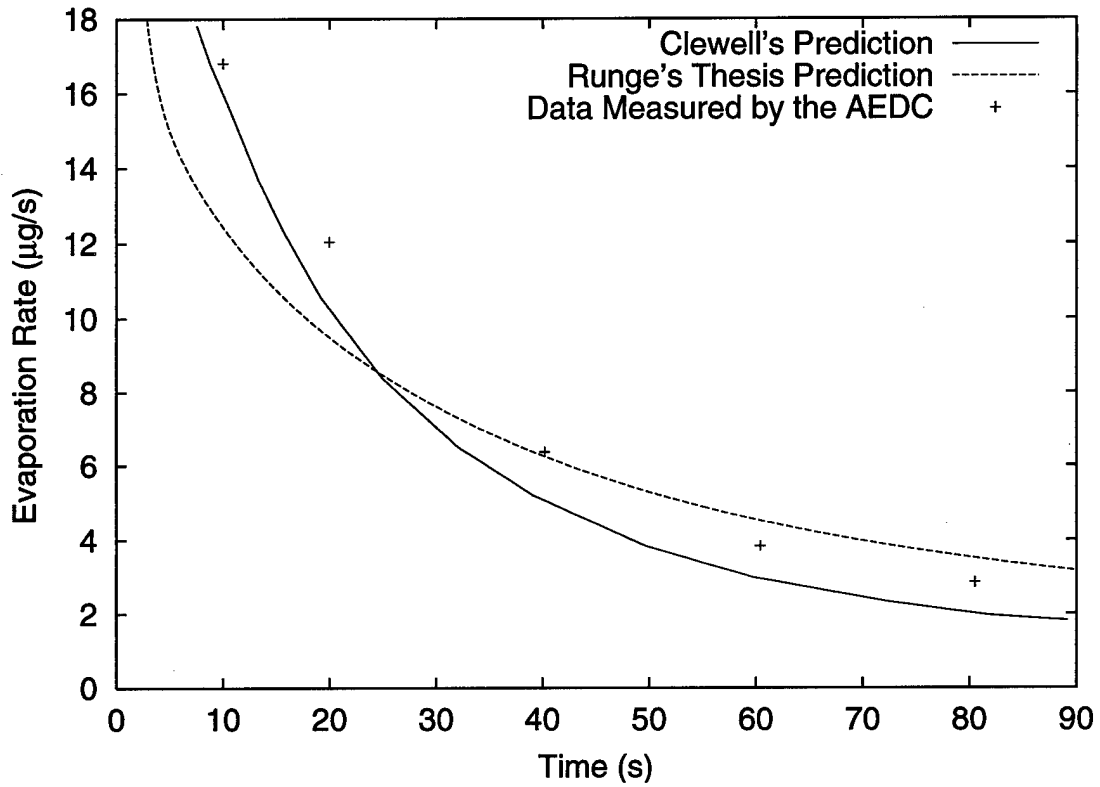
Figure 3.16   Comparison of calculations of Clewell and Runge's thesis equations compared to measured JP-4 evaporation rate. $T_\infty = 20^o$ C, $D_0 = 1347\mu m, u = 3m/s$.
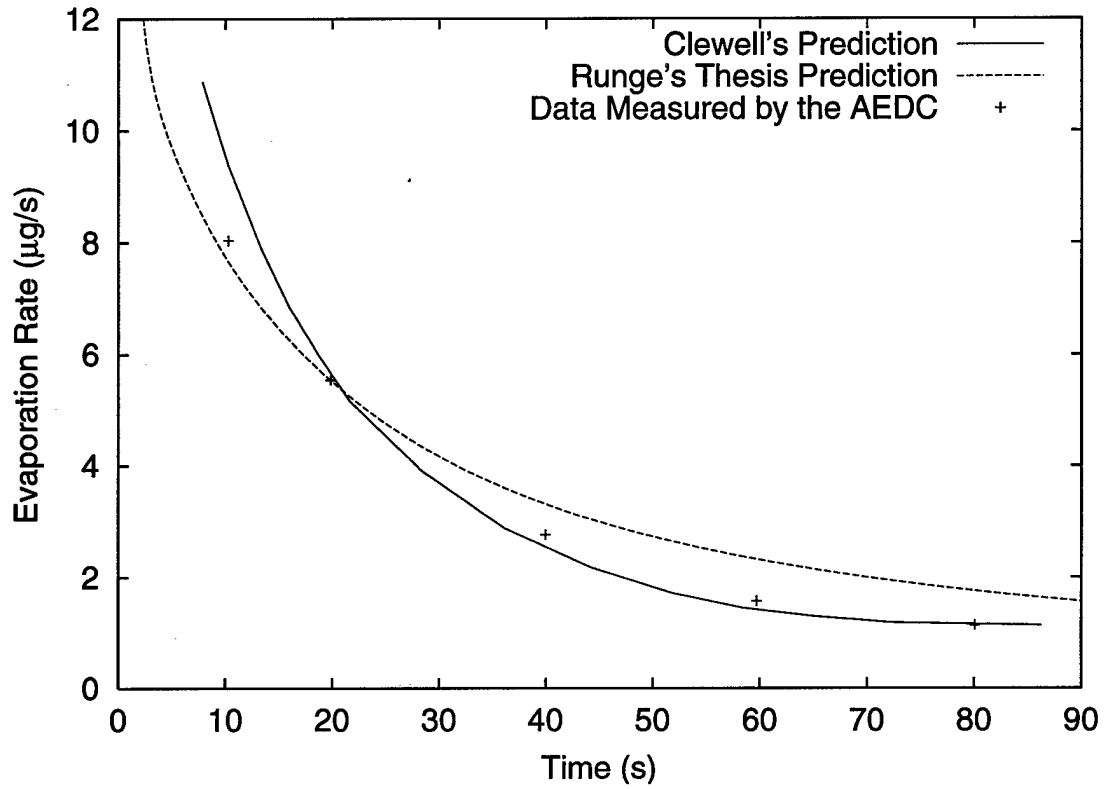
Figure 3.17   Comparison of calculations of Clewell and Runge's thesis equations compared to measured JP-4 evaporation rate. $T_\infty = 20^o$ C, $D_0 = 1060\mu m, u = 3m/s$.
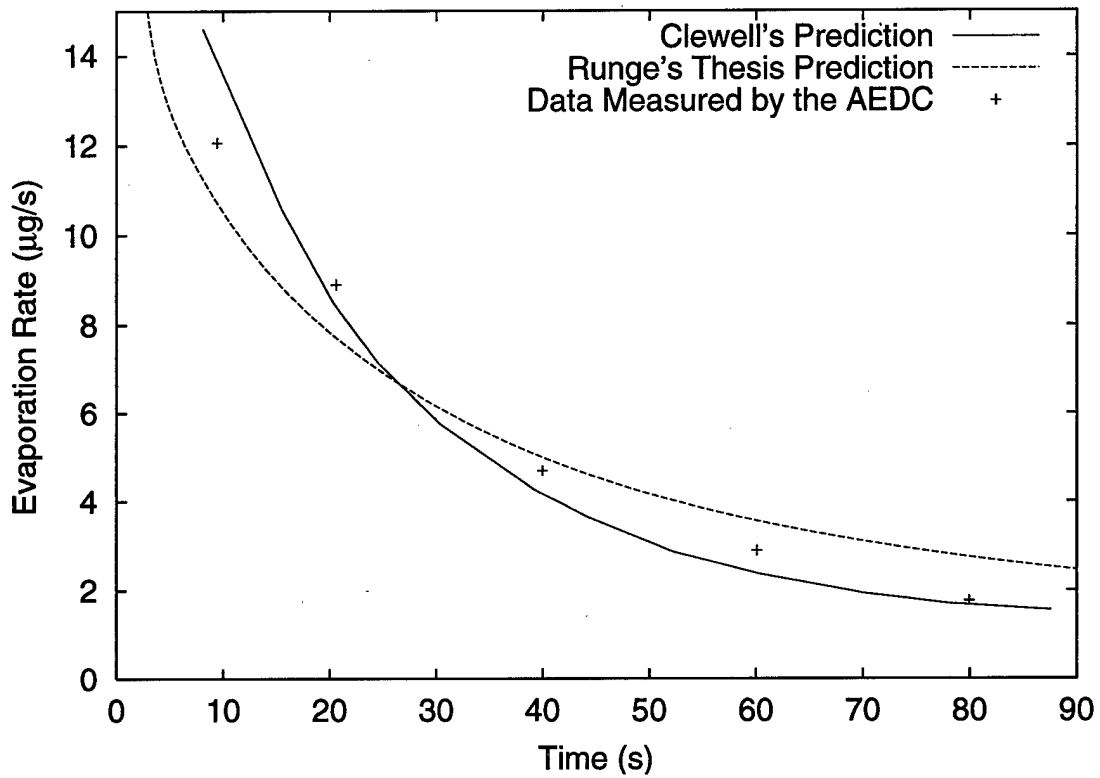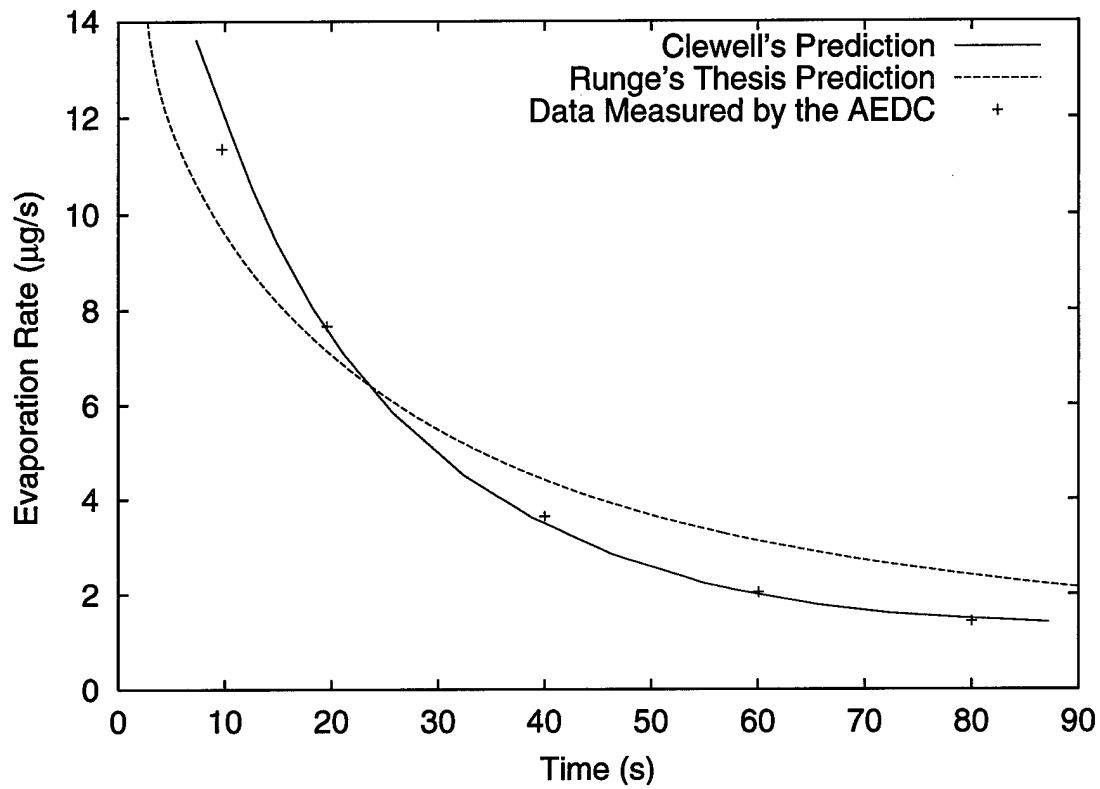
Figure 3.18   Comparison of calculations of Clewell and Runge's thesis equations compared to measured JP-4 evaporation rate. $T_\infty = 20^o$ C, $D_0 = 1179 \mu m, u = 3m/s$.

IV. Surface Evaporation

4.1 Overview

We consider the evaporation of fuel from a flat surface because, in toxicology studies, this flat surface could be the skin of ground crew exposed to the fuel.

4.2 Assumptions

- The surface from which the jet fuel is evaporating is flat.

- The surface is large enough that we only have to consider transport normal to the surface.

- The fuel does not penetrate the surface.

- The evaporating fuel is uniformly distributed in composition and temperature.

- Each species evaporates independently of the rest of the mixture.

- Air is insoluble in the fuel.

- The gas phase concentration of i at the surface of the fuel is the equilibrium vapor pressure of species i in the mixture.

- The vapor pressure of each species in the mixture follows Raoult's Law.

- The mixture of air and fuel gases at the surface of the liquid fuel form an ideal mixture.

- The concentration of fuel in the ambient airflow is zero.

Now we have simplified the problem in order to arrive at a close approximation to the solution. The validity of some of these assumptions needs to be considered.

The assumption that the skin can be represented by a flat surface may be improved by considering another shape, such as a cylinder. This consideration should be addressed in future work.

As a first approximation, the assumption that fuel species evaporate independently of the rest of the mixture is made as in Lowell (10). In section 4.3, we shall remove this assumption and consider the effects that the species mass transfer rates have on each other species. At that time, another assumption is made that the effective diffusivity is equal to the diffusivity in a binary mixture with air. This second assumption is justified when the diffusivity is only slightly position dependent (see reference (1)).

As described in the introduction, fuel is coming into contact with the ground crew. Assuming the concentration of fuel in the ambient airflow is zero may not be appropriate during the initial contact period. Therefore, this assumption is only valid after the addition of fuel to the skin has ceased.

4.3 Equations

Consider the heat transfer between the evaporating liquid fuel and the air. The heat is primarily transferred between the fuel and the air by the mechanisms of heat convection, q_c, and radiation, q_r. The convective heat flux is given as in equation (2.27) of section 2.2:

$$q_c = h\Delta T = h(T_\infty - T_F)$$

where h is the heat transfer coefficient, T_F is the temperature of the fuel, and T_∞ is the temperature of the approaching airflow. The heat transfer coefficient is given as equation (2.26) in section 2.2:

$$h = \frac{\kappa N_u}{L}$$

where κ is the thermal conductivity and N_u is the Nusselt number. The characteristic length scale, L, is the length of the surface along the direction of the ambient airflow.

The Nusselt number is a function of the Reynolds and Prandtl numbers. The coefficients are presented in reference (2) and were obtained through parameter fit-

ting experimental data:

$$N_u = 0.34 N_R^{1/2} N_P^{1/3}$$

The radiative heat flux is given by equation (2.31) in section 2.2:

$$q_r = \sigma(a_F T_\infty - e_F T_F)$$

where σ is the Stefan-Boltzmann constant, a_F is the absorptivity of the fuel, and e_F is the emmisivity of the fuel.

Heat is also lost through evaporative cooling, denoted q_h, as given in equation (2.32) in section 2.2:

$$q_h = \frac{\Delta H_{vap}}{A} \frac{dm}{dt}$$

where dm/dt is the change in mass with time, which will be a negative number, and ΔH_{vap} is the latent heat of vaporization. The product is divided by the area to give the evaporative heat loss per unit area per unit time. The total heat flux is the sum of these contributions:

$$q = q_c + q_r + q_h \tag{4.1}$$

The change in temperature with respect to time is given as in equation (2.40):

$$\frac{dT_F}{dt} = \frac{Aq}{mC_p} \tag{4.2}$$

where A is the surface area of the evaporating fuel, m is the total mass and C_p is the specific heat of the fuel.

Consider the mass transfer of a pure liquid, A, evaporating from a flat surface into a moving gas above the surface, B. The mass flux of gas A at the surface of liquid A is given by equation (2.10) in section 2.2:

$$n_{A0} = Y_{A0}(n_{A0} + n_{B0}) + k\Delta Y_A \tag{4.3}$$

where the definitions are the same as in section 2.2. Next, we follow the development in section 2.2 with one exception. The mass flux with respect to stationary coordinates is used so that the diffusion induced bulk flow term remains. Then subscripting this equations as in section 2.3.2, the time rate of change in mass of species i is given by:

$$\frac{dm_i}{dt} = \frac{Ak_iY_{i0}}{1 - Y_{i0}} \tag{4.4}$$

where A is the surface area. Notice that Y_{i0} and k_i are dependent on the fuel temperature.

The mass transfer coefficient is given by equation (2.13), $k = \rho \mathcal{D}_{ia} N_S / L$ where L is the length of the surface along the direction of the ambient airflow, and $\mathcal{D}_{ia}$ is the diffusivity of species i in air. The Sherwood number is an empirical fit to experimental measurement of mass transfer from a flat plate in a flowing liquid (see reference (2)). As was stated in section 2.2, it is a function of the Schmidt and Reynolds numbers:

$$N_S = 0.34 N_R^{1/2} N_c^{1/3}$$

Note that this equation for laminar flow over a flat surface differs from the equation (2.19), which is for laminar flow around a sphere.

The mass fraction of species i at the surface can be calculated as follows:

$$Y_{i0} = \frac{\chi_{i0}w_i}{\sum_{j=1}^{N} \chi_{j0}w_j + \chi_{a0}w_a}$$

where χ_{a0} and w_a are the mole fraction at the surface and molecular weight of air, respectively. Then, as we have assumed, the mole fraction of i at the surface is equal to the equilibrium concentration:

$$\chi_{i0} = \frac{P_{i,vap}}{P_0}$$

4-4

where $P_{i,vap}$ is the vapor pressure of species i in the mixture and P_0 is the total pressure at the surface. The vapor pressure of species i is calculated using Raoult's Law, equation (2.35):

$$P_{i,vap} = \chi_i^\ell P_{i,vap}^0$$

where the superscripts zero denotes pure i and the ℓ denotes the liquid phase.

The assumption that each species' evaporation rate is independent of the rest of the species' evaporation rates can be discarded. Then, as presented in reference (1), the multicomponent mass flux of species i due to ordinary diffusion is conveniently given in terms of the multicomponent diffusivity of i in an ideal mixture with the other N species:

$$\mathbf{n}_i = -\rho \mathcal{D}_{im} \nabla Y_i + Y_i \sum_{j=1}^{N} \mathbf{n}_j \quad . \tag{4.5}$$

Since we are still assuming that the surface is long enough that diffusion in the y-z plane, parallel to the surface, is negligible, the vector equation (4.5) simplifies to a one-dimensional equation:

$$n_i = -\rho \mathcal{D}_{im} \Delta Y_i + Y_i \sum_{j=1}^{N} n_j$$

where ΔY is the composition difference in the direction normal to the surface. Evaluating this equation at the surface and denoting this with the subscript zero, the equation for the mass flux at the surface of the evaporating fuel is:

$$n_{i0} = -\rho \mathcal{D}_{im} \Delta Y_i + Y_{i,0} \sum_{j=1}^{N} n_{j0}$$

Then, multiplying through by the surface area of the fuel yields the evaporation rate of species i:

$$\frac{dm_i}{dt} = Y_{i,0} \sum_{j=1}^{N} \frac{dm_j}{dt} - A\rho \mathcal{D}_{im} \Delta Y_i \tag{4.6}$$

where the area is the length times the width of the fuel on the surface.

4-5

Rearranging this equation to get the derivative terms on the left-hand side results in:

$$\frac{dm_i}{dt} - Y_{i,0} \sum_{j=1}^{N} \frac{dm_j}{dt} = -A\rho \mathcal{D}_{im} \Delta Y_i$$

Bringing dm_i/dt out of the summation and substituting $\Delta Y_i = Y_{i,0} - Y_{i,\infty} = Y_{i,0}$ leads to:

$$(1 - Y_{i,0})\frac{dm_i}{dt} - Y_{i,0} \sum_{j=1,j\neq i}^{N} \frac{dm_j}{dt} = -A\rho \mathcal{D}_{im} Y_{i,0}$$

Dividing through by Y_{i0} yields:

$$\frac{1 - Y_{i,0}}{Y_{i,0}} \frac{dm_i}{dt} + \sum_{j=1,j\neq i}^{N} \frac{dm_j}{dt} = -A\rho \mathcal{D}_{im}$$

This can be set up and solved as a matrix equation of the form:

$$B \frac{d\mathbf{m}_i}{dt} = \rho \mathcal{D} \tag{4.7}$$

where B is the matrix of the coefficients is:

$$B = \begin{pmatrix} (1 - Y_{1,0})/Y_{1,0} & 1 & \cdots & 1 \\ 1 & (1 - Y_{2,0})/Y_{2,0} & \cdots & 1 \\ \vdots & \vdots & \vdots & \vdots \\ 1 & 1 & \cdots & (1 - Y_{N,0})/Y_{N,0} \end{pmatrix}$$

Equations (4.4) and (4.7) have been implemented for comparison to the experimental data below.

To describe the mass flux due to evaporation of fuel from a surface, equations (4.4) or (4.7) are appropriate. The mass flux with respect to mass average velocity, j_i, should not be used to describe the evaporation from a flat surface. The mass average velocity in the surface evaporation system would be moving away from the surface since it has been assumed that no mass is moving through the surface. As we

are interested in the mass flux at the surface and do not want to obtain a solution away from the surface, we must use n_i.

When applied to the problem of evaporation of fuel from skin, the assumption that no mass is transported through the surface is not valid. Dermal absorption does occur and this problem may be handled by also computing the dermal absorption rate of the fuel through the skin.

4.4 Comparison to Experimental Data

Evaporation of Arctic Diesel 40, a No. 2 fuel oil, has been measured by Regnier and Scott (14). A dark evaporation chamber provided a constant ambient airflow of 21 km/hr and allowed the ambient temperature to be adjusted to 5, 10, 20, and 30 degrees C. Note that the high ambient flow velocity used in this experiment is more characteristic of the ambient flow velocity encountered during a cold start situation. The vaporized fuel was removed from the air stream by using a water aspirator at the exhaust outlet. Samples of oil weighing 12 ± 7 grams were measured into 90 mm diameter Petri dishes and then placed in the chamber and weighed periodically. The oil depth was approximately 3 mm for each case.

We wish to determine if the flat surface evaporation model predicts the evaporation of fuel from a flat surface more accurately than the droplet evaporation models. Therefore, the experimental measurements of the percentage of initial mass of oil remaining are compared to the flat surface evaporation model and Clewell's droplet evaporation model.

For the flat surface evaporation simulations, the surface area of the fuel in the circular Petri dish was computed as $A = \pi r^2 = \pi(0.9)^2, cm^2$. The fuel mass was set equal to 12.0 g to match the experimental conditions.

For the spherical droplet evaporation simulations, the diameter was calculated from the initial droplet mass, which was set equal to 12.0 g. The volume of the

droplet was then calculated using:

$$V = \frac{m}{\rho}$$

where m is the mass of the droplet and it was assumed that the density of the droplet, ρ, was equal to the sum of the densities of each component of the fuel. The volume of a spherical droplet is given by:

$$V = \frac{4}{3}\pi r^3$$

which was solved for r to obtain the droplet radius required to result in the given droplet mass.

The fuel oil composition from reference (14) is used for the simulations and is shown in table 4.1. The species listed were obtained by chromatography and only account for 18% of the mixture. However, it is hypothesized by Regnier and Scott that the composition listed in table 4.1 is sufficient for characterizing the evaporative behavior of the oil. This follows from the assumption that the components that are lighter than nonane will evaporate very quickly and components that are heavier than octadecane will evaporate very little.

Species	Volume Fraction	Molecular Weight	Boiling Point, K	Density at 20° C, kg/m^3
C-9	0.039	128.3	415.15	720.0
C-10	0.103	142.3	433.15	720.0
C-11	0.150	156.3	469.15	740.0
C-12	0.154	170.3	489.15	750.0
C-13	0.155	184.4	508.15	760.0
C-14	0.158	198.4	527.15	760.0
C-15	0.107	212.4	544.15	770.0
C-16	0.073	226.4	560.15	770.0
C-17	0.044	240.4	575.20	778.0
C-18	0.019	254.4	589.25	777.0

Table 4.1   Arctic Diesel 40 characterization

Figures 4.1, 4.2, 4.3, and 4.4 are the comparisons of the predictions of the flat surface model and Clewell's droplet evaporation model to the experimental measurements of the percent of initial mass remaining at 30° C, 20° C, 10° C, and 5° C, respectively. The thermodynamic properties used for the predictions are obtained using the empirical relations for hydrocarbons that are derived by Clewell in reference (3).

The predictions of the flat surface evaporation model are in reasonably good agreement with the measured data. For the higher temperatures though, the flat surface model predictions of the mass evaporated are too high at later times. Although the initial surface area and mass are equivalent for the droplet and the fuel in the circular Petri dish, the droplet evaporation predictions are poor. The Sherwood number, N_s, is computed in the droplet model by:

$$N_s = 2.0 + 0.6 N_R^{1/2} N_c^{1/3}$$

while N_s is computed by the flat surface model by:

$$N_s = 0.34 N_R^{1/2} N_c^{1/3}$$

Given the differences in the calculations of the Sherwood numbers, and therefore the mass transfer coefficients, we would expect the droplet model to predict evaporation rates that are too large.

At large times, the predictions of the flat surface model at the two lower temperatures (figures 4.3 and 4.4) are in closer agreement with the measurements than the predictions at the higher temperatures (figures 4.1 and 4.2). At small times, the predictions at the two higher ambient temperatures are closer to the experimental measurements than the predictions at the lower ambient temperatures. When the temperature is 5 degrees Celsius, the surface evaporation model under-predicts the
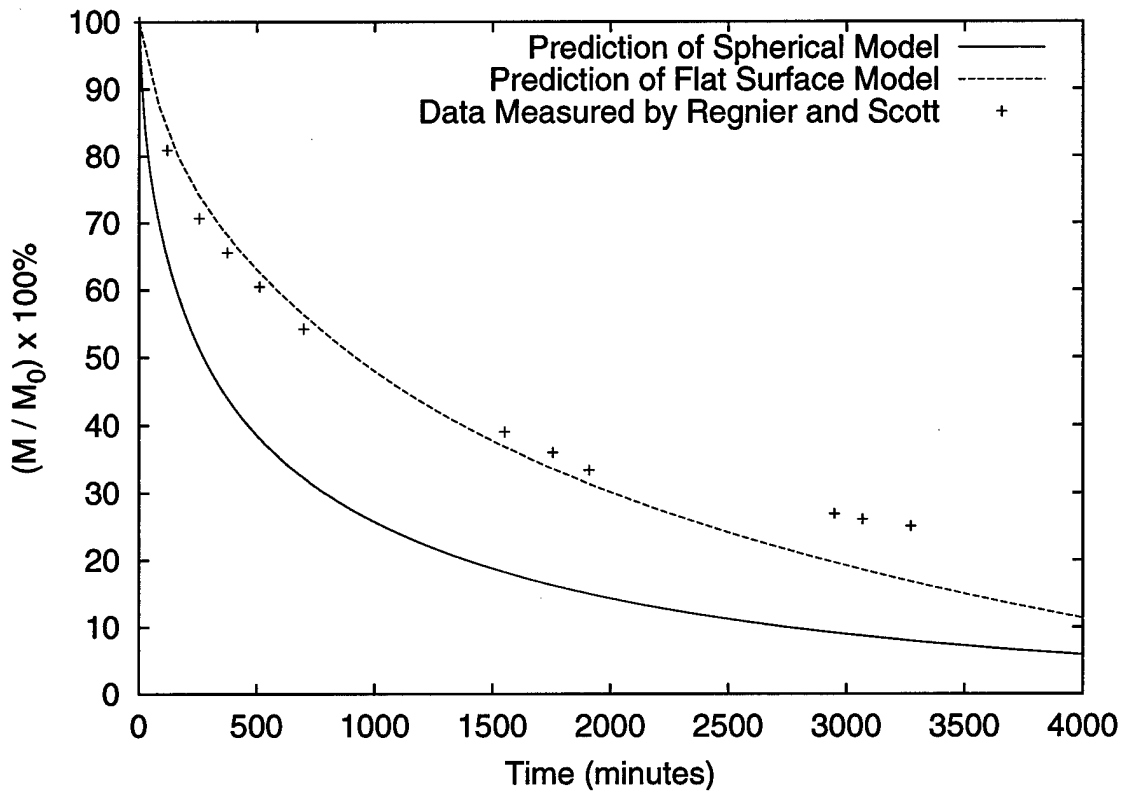
4-9

Figure 4.1   Comparison of predictions of percentage of initial mass of oil remaining
to experimentally measured values at $T = 30^o$ C.

amount of fuel evaporated by as much as 5% in the mid-stages of the simulation,
and then comes close to the measured mass again at later times.

The error in the flat surface model's predictions of the mass remaining may be
because we have assumed that we have a flat plate wetted with fuel. However, the
experimental data is the measurement of the evaporation of the fuel from inside of a
Petri dish. As the fuel evaporates, the fuel surface falls below the edges of the dish,
which would affect the flow of air across the surface. Secondly, the air velocity is very
high, producing a Reynolds number on the order of 3.0 x 10^5 which indicates that
we are in the transition regime. Turbulent effects, which have not been modeled,
are likely affecting the evaporation rate. Another possible explanation is that the
predicted fuel temperature is higher than the actual temperature. We have followed
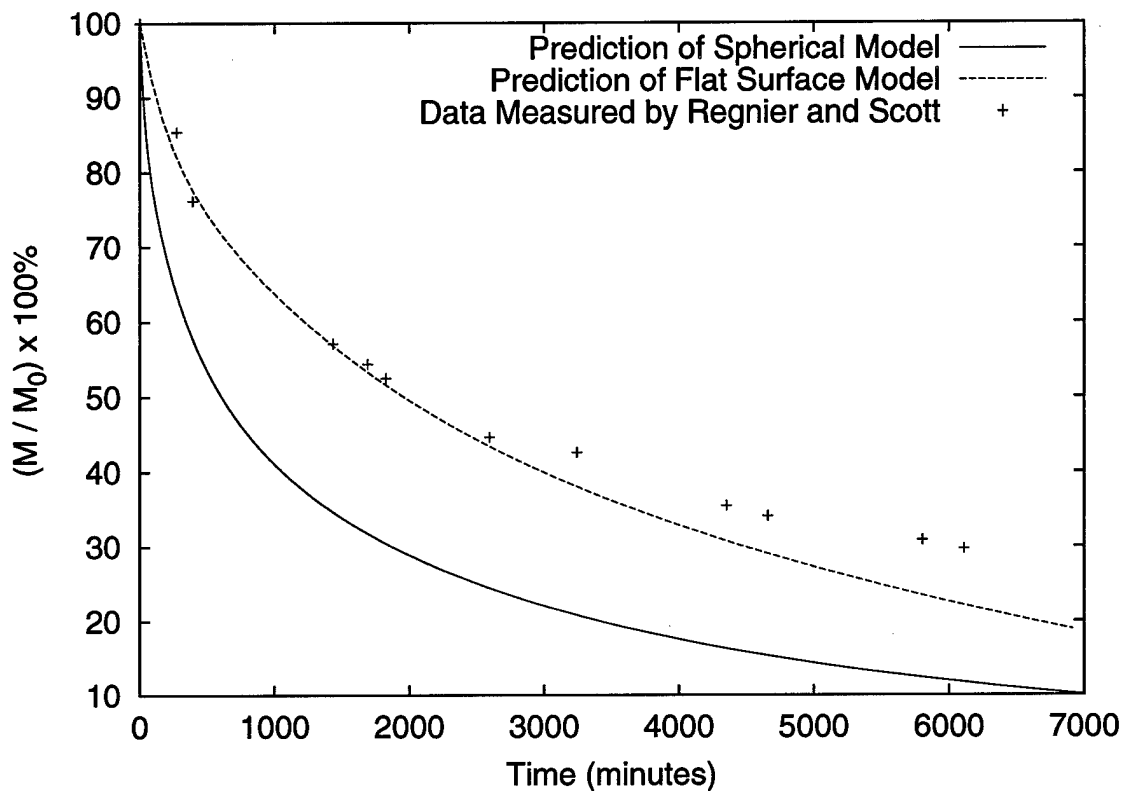
Figure 4.2   Comparison of predictions of percentage of initial mass of oil remaining
to experimentally measured values at $T = 20^o$ C.

the approach of Clewell which uses empirical relations for hydrocarbons that air
fairly general. However, the linear formula for the latent heat of vaporization was
derived by Clewell from inspection of the heats of vaporization for the range of
hydrocarbons that are in JP-4. JP-4 is composed of several hydrocarbons that are
lighter than those listed in table 4.1, which may lead to a relationship for the latent
heat that is too small. This could lead underestimating the amount of evaporative
cooling, producing temperature predictions that are too high. In addition, the higher
temperatures would increase the error in Clewell's approach for predicting the latent
heat of vaporization. Without measured temperature data, this cannot be confirmed
though.
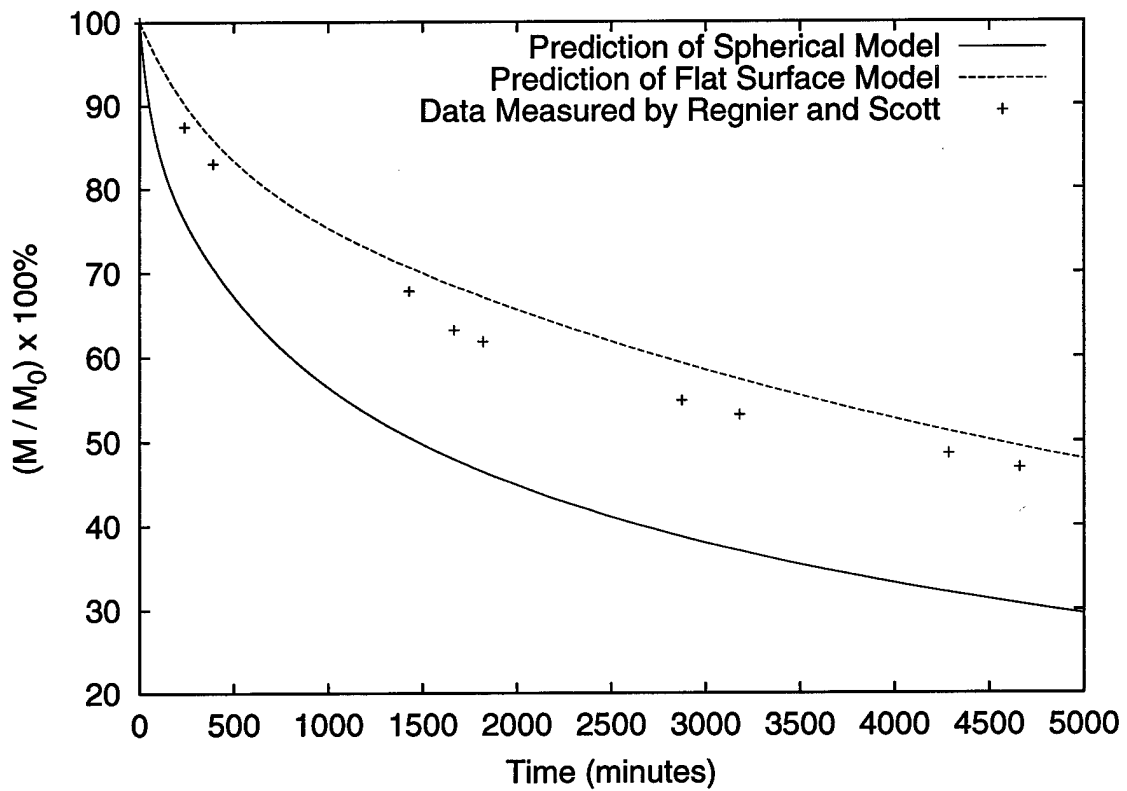
Figure 4.3   Comparison of predictions and measurements of percentage of initial
mass of oil remaining at $T = 10^o$ C.

It should be noted here that Regnier and Scott developed an activation energy
evaporation model (14). The predictions of their model were more accurate than
both the flat surface or spherical model discussed earlier. This suggests that an
activation energy approach to calculating the evaporation of fuel from skin should
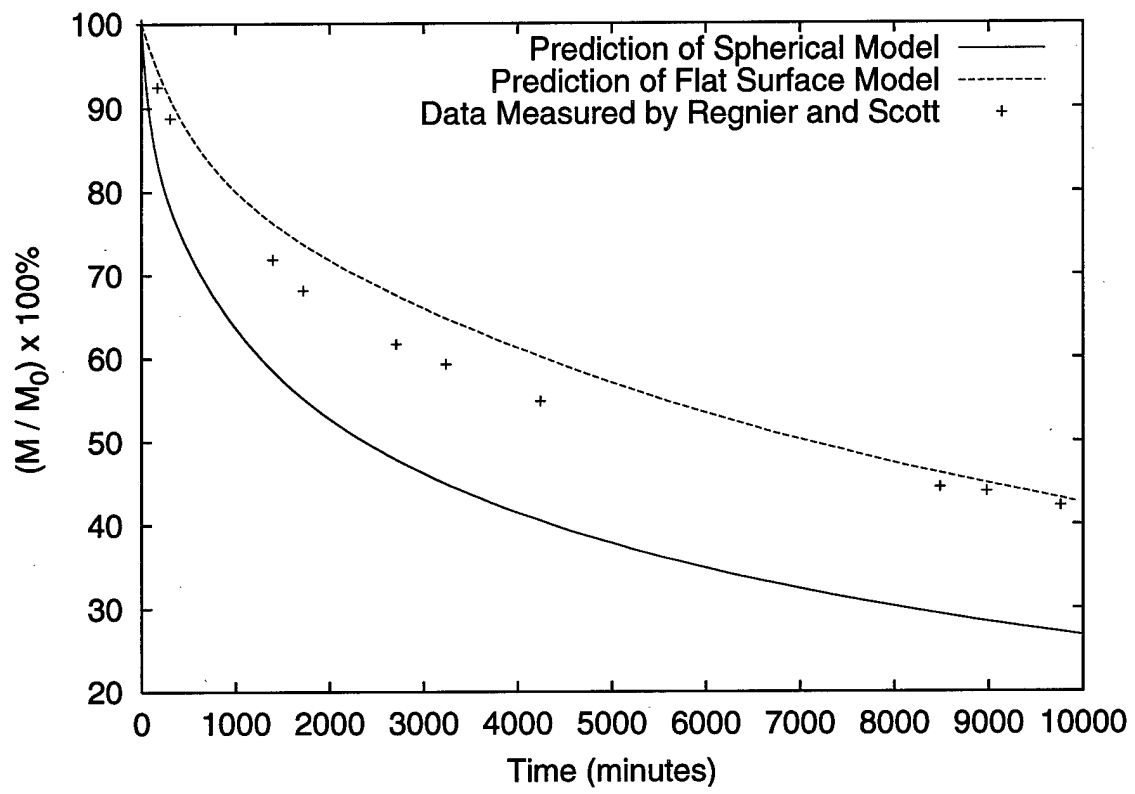be considered in future work.

Figure 4.4   Comparison of predictions and measurements of percentage of initial mass of oil remaining at $T = 5^o$ C.

V. Summary and Conclusions

5.1 Summary

For this research, two previously developed fuel droplet evaporation models were compared and the equations to describe surface fuel evaporation were developed in order to predict evaporation of fuel from skin following exposure. The equations of the two previous algorithms were shown to be derived from basic principles of heat and mass transfer and the predictions were compared to experimental laboratory data. The surface evaporation equations were then derived from those basic principles, following the approach of Clewell, and its predictions of the surface evaporation was compared to experimental data. This research resulted in a computer program that may be used to predict the evaporation of fuel from a surface. The surface evaporation algorithm can be used in conjunction with a program that predicts the dermal absorption of fuel to determine the dose of fuel delivered to the exposed ground crew workers.

5.2 Conclusions

The two previous descriptions produce predictions that agree very well with their respective sets of experimental data. However, the predictions presented in reference (16) could not be reproduced from the equations shown in the appendix of reference (16). If the problem with the inconsistent notation used to present the equations is resolved and the predictions that appear in the article can be reproduced, then the approach of Runge et al. produce more accurate predictions of JP-4 and JP-8 evaporation than the approach of Clewell. The equations used in Runge's thesis (reference (17)) may be used to produce results that match those of reference (16) almost exactly.

In terms of adapting to meet the changing needs of the Air Force through the modeling of new aircraft fuels, the approach of Clewell is superior. The only exper-

iments which must be performed to model a new hydrocarbon fuel using Clewell's approach is one to ascertain the predominant species with which to characterize the fuel's behavior. It has already been partly demonstrated by the predictions of the evaporation of the Arctic Diesel 40 that this approach is robust while producing reasonably accurate results. Next, the fuel specific correlations for the thermodynamic properties, such as the specific heat and latent heat, could be recalculated using data that can be found in the literature. To model the evaporation of a new fuel using the approach of Runge et al., one would have to perform several evaporation experiments in order to obtain constants for use in the calculation of the $\rho \mathcal{D}$ product.

The calculations of the algorithm are within 5% of the measured mass remaining for temperatures of 5 and 10 degrees Celsius using a 10 species characterization of the fuel that accounted for approximately 18% of the actual fuel oil mixture. For higher temperature vaporization, the surface evaporation algorithm reproduced the experimental data to within 10% mass remaining for temperatures of 20 and 30 degrees Celsius.

5.3 Recommendations for Further Research

Further research into the evaporation of jet fuel from skin is needed. It remains to be determined if the approximation of the skin as a flat surface is a good assumption, or if there is a better geometry such as a cylinder. Secondly, the performance of the model in high ambient flow velocities, such as those encountered during cold start, has been investigated in chapter IV. However, turbulent effects at the high ambient flow velocity should be considered in future work.

The activation energy approach used by Regnier and Scott (14) produced more accurate predictions of the mass evaporated than the other models compared. Research into an activation energy approach to calculating the evaporation of fuel from skin should be conducted.

Bibliography

1. Bird, Steward and Lightfoot. *Transport Phenomena* (Second Edition). New York: Wiley, 1960c,1962.

2. Clark, M. *Transport modeling for environmental engineers and scientists* (First Edition). New York: Wiley, 1996.

3. Clewell, H. J. *Evaporation and Groundfall of JP-4 Jet Fuel Jettisoned by USAF Aircraft*. Technical Report ELS-TR-80-56, Air Force Engineering and Services Center, September 1980.

4. Dawbarn, R., K. W. Nutt and C. W. Pender. *A Study of the Jettisoning of JP-4 Fuel in the Atmosphere*. Technical Report AEDC-TR-75-49, Arnold Engineering Development Center, November 1975.

5. Fuchs, N. A. *Evaporation and droplet growth in gaseous media*. New York: Pergamon press, 1959.

6. Glassman, I. *Combustion* (Second Edition). Orlando: Harcourt Brace Jovanovich, 1987.

7. Incropera, F. P. and D. P. De Witt. *Fundamentals of Heat and Mass Transfer* (Second Edition). New York: Wiley, 1985.

8. Kuo, K. K. *Principles of Combustion*. New York: Wiley, 1986.

9. Law, C. K. "Multicomponent Droplet Combustion with Rapid Internal Mixing," *Combustion and Flame, 26*:219–233 (1976).

10. Lowell, H. *Free Fall and Evaporation of JP-4 Jet Fuel Droplets in a Quiet Atmosphere*. Technical Report NASA-TN-D-33, National Aeronautics and Space Administration, September 1959.

11. Lowell, H. *Free Fall and Evaporation of JP-1 Jet Fuel Droplets in a Quiet Atmosphere*. Technical Report NASA-TN-D-199, National Aeronautics and Space Administration, 1960.

12. Pfeiffer, K. D. *A Numerical Model to Predict the Fate of Jettisoned Aviation Fuel*. MS thesis, Air Force Institute of Technology Graduate School of Engineering, 1994.

13. Pfieffer, K. D., D. W. Quinn and C. E. Dungey. "Numerical Model to Predict the Fate of Jettisoned Aviation Fuel," *Journal of Aircraft, 33, Number 2*:353–362 (1996).

14. Regnier, Z. and B. Scott. "Evaporation Rates of Oil Components," *Environmental Science and Technology, 9*:469–472 (1975).

15. Reid, R., J. Prausnitz and T. Sherwood. *The Properties of Gases and Liquids* (Third Edition). New York: McGraw-Hill Book Company, 1977.

16. Runge, T., M. Teske and C. E. Polymeropoulos. "Low-Temperature Vaporization of JP-4 and JP-8 Fuel Droplets," *Atomization and Sprays*, *8*:25–44 (1998).

17. Runge, T. H. *Vaporization of Droplets Formed After Fuel Jettisoning from Aircraft*. MS thesis, Rutgers University, 1996.

18. Williams, F. A. *Combustion Theory*. Reading, Massachusetts: Addison - Wesley, 1965.

1. AGENCY USE ONLY *(Leave blank)*	2. REPORT DATE September 1999	3. REPORT TYPE AND DATES COVERED Master's Thesis

4. TITLE AND SUBTITLE
EVAPORATION OF JET FUELS

5. FUNDING NUMBERS
QAF185995203001

6. AUTHOR(S)
Charles Eric Hack, AD-21 AFOSR/NL

7. PERFORMING ORGANIZATION NAME(S) AND ADDRESS(ES)
Air Force Institute of Technology
2950 P Street
WPAFB OH 45433-7765

8. PERFORMING ORGANIZATION REPORT NUMBER

AFIT/GES/ENC/99S-01

9. SPONSORING/MONITORING AGENCY NAME(S) AND ADDRESS(ES)
Dr. Walter Kozumbo
801 North Randolph Street, Room 732
Arlington, VA 22203-1977

10. SPONSORING/MONITORING AGENCY REPORT NUMBER

11. SUPPLEMENTARY NOTES
Dr. Dennis W. Quinn, ENC

12a. DISTRIBUTION AVAILABILITY STATEMENT
APPROVED FOR PUBLIC RELEASE; DISTRIBUTION UNLIMITED

12b. DISTRIBUTION CODE

13. ABSTRACT *(Maximum 200 words)*
As part of the start-up procedures for jet engines, fuel is passed through aircraft engines before combustion is initiated. Because of the extremely low temperatures at northern tier Air Force bases, the unburned fuel does not evaporate readily and may come into contact with ground crew. To determine the amount and duration of contaminant contact, the evaporation of the emitted fuel must be modeled. The amount and composition of the fuel upon reaching the ground crew may be determined by droplet evaporation models that have already been developed. The evaporation of the fuel after adhering to the skin needs to be modeled. This knowledge of the fuel's fate may then be used to determine source terms for use in toxicological studies.

This research involves the comparison of two existing droplet evaporation models and the calculation of the evaporation of a film of jet fuel from a flat surface. The existing models are compared in order to make recommendations on which model to use to predict the amount and composition of fuel reaching the ground crew. To make the surface evaporation problem amenable to modeling, simplifying assumptions are made.

The goal of this research is to determine the most appropriate model for predicting the amount and composition of jet fuel reaching the ground crew and to extend the more appropriate fuel droplet evaporation model to describe the evaporation of a film of fuel from a surface. A validation of the resultant model is then performed by comparing the calculations to experimental data.

14. SUBJECT TERMS
Evaporation, Vaproization, Aviation Fuels, Jet Engine Fuels, Fuel Contamination

15. NUMBER OF PAGES
86

16. PRICE CODE

17. SECURITY CLASSIFICATION OF REPORT	18. SECURITY CLASSIFICATION OF THIS PAGE	19. SECURITY CLASSIFICATION OF ABSTRACT	20. LIMITATION OF ABSTRACT
Unclassified	Unclassified	Unclassified	UL

GENERAL INSTRUCTIONS FOR COMPLETING SF 298

The Report Documentation Page (RDP) is used in announcing and cataloging reports. It is important that this information be consistent with the rest of the report, particularly the cover and title page. Instructions for filling in each block of the form follow. It is important to *stay within the lines* to meet *optical scanning requirements.*

Block 1. Agency Use Only *(Leave blank)*.

Block 2. Report Date. Full publication date including day, month, and year, if available (e.g. 1 Jan 88). Must cite at least the year.

Block 3. Type of Report and Dates Covered. State whether report is interim, final, etc. If applicable, enter inclusive report dates (e.g. 10 Jun 87 - 30 Jun 88).

Block 4. Title and Subtitle. A title is taken from the part of the report that provides the most meaningful and complete information. When a report is prepared in more than one volume, repeat the primary title, add volume number, and include subtitle for the specific volume. On classified documents enter the title classification in parentheses.

Block 5. Funding Numbers. To include contract and grant numbers; may include program element number(s), project number(s), task number(s), and work unit number(s). Use the following labels:

C - Contract	**PR** - Project
G - Grant	**TA** - Task
PE - Program	**WU** - Work Unit
Element	Accession No.

Block 6. Author(s). Name(s) of person(s) responsible for writing the report, performing the research, or credited with the content of the report. If editor or compiler, this should follow the name(s).

Block 7. Performing Organization Name(s) and Address(es). Self-explanatory.

Block 8. Performing Organization Report Number. Enter the unique alphanumeric report number(s) assigned by the organization performing the report.

Block 9. Sponsoring/Monitoring Agency Name(s) and Address(es). Self-explanatory.

Block 10. Sponsoring/Monitoring Agency Report Number. *(If known)*

Block 11. Supplementary Notes. Enter information not included elsewhere such as: Prepared in cooperation with....; Trans. of....; To be published in.... When a report is revised, include a statement whether the new report supersedes or supplements the older report.

Block 12a. Distribution/Availability Statement. Denotes public availability or limitations. Cite any availability to the public. Enter additional limitations or special markings in all capitals (e.g. NOFORN, REL, ITAR).

DOD -	See DoDD 5230.24, "Distribution Statements on Technical Documents."
DOE -	See authorities.
NASA -	See Handbook NHB 2200.2.
NTIS -	Leave blank.

Block 12b. Distribution Code.

DOD -	Leave blank.
DOE -	Enter DOE distribution categories from the Standard Distribution for Unclassified Scientific and Technical Reports.
NASA -	Leave blank.
NTIS -	Leave blank.

Block 13. Abstract. Include a brief *(Maximum 200 words)* factual summary of the most significant information contained in the report.

Block 14. Subject Terms. Keywords or phrases identifying major subjects in the report.

Block 15. Number of Pages. Enter the total number of pages.

Block 16. Price Code. Enter appropriate price code *(NTIS only)*.

Blocks 17. - 19. Security Classifications. Self-explanatory. Enter U.S. Security Classification in accordance with U.S. Security Regulations (i.e., UNCLASSIFIED). If form contains classified information, stamp classification on the top and bottom of the page.

Block 20. Limitation of Abstract. This block must be completed to assign a limitation to the abstract. Enter either UL (unlimited) or SAR (same as report). An entry in this block is necessary if the abstract is to be limited. If blank, the abstract is assumed to be unlimited.